University of Washington
Department of Civil and Environmental Engineering

PREDICTION OF SEDIMENT EROSION AND TRANSPORT WITH THE DISTRIBUTED HYDROLOGY-SOIL-VEGETATION MODEL

COLLEEN O. DOTEN
and
DENNIS P. LETTENMAIER

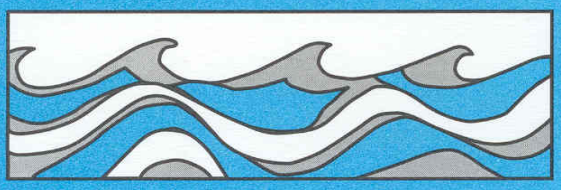

Water Resources Series
Technical Report No.178
August 2004

Seattle, Washington
98195

Department of Civil Engineering
University of Washington
Seattle, Washington 98195

PREDICTION OF SEDIMENT EROSION AND TRANSPORT WITH THE DISTRIBUTED HYDROLOGY-SOIL-VEGETATION MODEL

COLLEEN O. DOTEN
and
DENNIS P. LETTENMAIER

Water Resources Series
Technical Report No. 178

August 2004

ABSTRACT

Erosion and sediment transport in a temperate forested watershed are predicted with a new sediment module linked to the Distributed Hydrology-Soil-Vegetation Model (DHSVM). The DHSVM sediment module represents the main sources of sediment generation in forested environments: mass wasting, hillslope erosion and road surface erosion. It produces failures based on a factor-of-safety analysis with the infinite slope model through use of stochastically generated soil and vegetation parameters. Failed material is routed downslope with a rule-based scheme that determines sediment delivery to streams. Sediment from hillslopes and road surfaces is also transported to the channel network. A simple channel routing scheme is implemented to predict basin sediment yield. We demonstrate through an initial application of this model to the Rainy Creek catchment, a tributary of the Wenatchee River which drains the east slopes of the Cascade Mountains, that the model produces plausible sediment yield and ratios of landsliding and surface erosion, when compared to published rates for similar catchments in the Pacific Northwest.

TABLE OF CONTENTS

LIST OF FIGURES

LIST OF TABLES

ACKNOWLEDGEMENTS

We wish to express sincere gratitude to others who contributed to the development of the DHSVM sediment module. Laura C. Bowling developed the initial mass wasting and surface erosion algorithms. Edwin P. Maurer developed the initial channel routing algorithm. Jordan S. Lanini tested and improved the surface erosion and channel routing algorithms. Financial support was provided by the United States Department of Agriculture Forest Service Pacific Northwest Research Station and Wenatchee Forestry Sciences Laboratory.

The first author wishes to thank Derek B. Booth and David R. Montgomery for the improvements to this thesis that resulted from their careful reading of earlier versions. A special thanks is due to Laura C. Bowling with whom discussions and other model development support were extremely beneficial and tremendously appreciated.

In addition, thanks are due to Kristen Bergen for his efforts in completing the aerial photograph landslide survey, Ted Bohn for his coding and debugging assistance and to past and present members of the Land Surface Hydrology group at the University of Washington for their efforts and guidance.

1. INTRODUCTION

The effect of forest disturbance and management on aquatic resources in mountainous terrain is a problem of considerable contemporary scientific and public concern. The relationship between land use and erosion in mountainous forested watersheds has been known in a qualitative sense for some time. Vegetation management, forest road construction and forest fires impact basin sediment yield by increasing the amount of sediment available for transport and the amount of surface water available to transport it. Vegetation removal increases rates of surface erosion and mass wasting, temporarily until vegetation is re-established or permanently depending on the type of vegetation that establishes. Forest roads affect basin hydrology and mass wasting through interception and redirection of subsurface flow, and they are another source of surface sediment in these environments.

Various predictive models have been developed to assess the effects of forest management on sediment generation and transport. One of the earliest, the empirically based Universal Soil Loss Equation (USLE), was developed to provide estimates of average annual sediment yield for agricultural applications. It has since been applied to a wide variety of land use types, including burned forests (Gonzalez-Bonorino and Osterkamp, 2004). The more complex process-based Water Erosion Prediction Project model (WEPP; Ascough et al., 1997) was created to address shortcomings in the empirically based USLE. However, neither USLE nor WEPP account directly for the processes, such as shallow landsliding, that dominate sediment mobilization in forested watersheds in the western United States (Dietrich and Dunne, 1978; Wu and Sidle, 1995). For regions where shallow landsliding dominates, a number of subsequent slope-stability prediction tools have been developed and applied. Hazard mapping tools based on the infinite slope model linked with steady-state representations of subsurface flow and/or soil moisture have been pursued by a number of researchers (e.g., Ward et al., 1982; Hammond et al., 1992; Montgomery and Dietrich, 1994; Borga et al., 2002). Other approaches in this general category include dSLAM (Wu and Sidle, 1995) and IDSSM (Dhakal and Sidle, 2003) which are slope stability models that incorporate relatively simple representations of dynamic hydrology, instead of steady-state representations. While these models can be used for risk assessment, they generally only address failure initiation and not failure runout or sediment delivery to channels.

Also, these models do not incorporate the dynamic hydrology that, in addition to triggering mass wasting events, drive surface erosion and sediment routing.

A somewhat different approach to predicting sediment movement in forested watersheds derives from spatially distributed, physically-based hydrologic models. The initial purpose of these models was to predict streamflow and runoff. It has been a somewhat natural step to extend these models to predict the movement of various waterborne constituents, including sediment. In order to represent the runoff generation process, these models also represent various aspects of spatial and temporal variability in some of the factors controlling slope stability and other erosional processes. SHETRAN/SHESED (Wicks and Bathurst, 1996; Burton and Bathurst, 1998), built on the System Hydrologique European (SHE) hydrology model, is one example. It represents surface erosion, mass wasting (deterministically by predicting failure locations with mean soil and vegetation parameters), sediment delivery to channels and channel routing. However, an approach that includes forest roads, their effects on basin hydrology and mass wasting and erosion of road surfaces, as well as routing of eroded sediment to and through the channel network has yet to be developed.

In this thesis, we describe an approach for estimating sediment delivery and channel transport in mountainous forested watersheds typical of the Pacific Northwest (PNW) that addresses shortcomings in existing methods for prediction of effects of forest management and disturbance regimes on sediment generation. The approach is based on the existing Distributed Hydrology-Soil-Vegetation Model (DHSVM) construct (Wigmosta et al., 1994; Wigmosta and Lettenmaier, 1999). DHSVM is a spatially distributed hydrological model that explicitly represents the effects of topographic and subsurface heterogeneities on the downslope redistribution of subsurface moisture. It was designed to provide a physically-based tool to address the hydrologic consequences, especially changes in flood potential, associated with forest disturbance (logging, fire, forest roads) in forested mountainous watersheds. DHSVM has been applied to a number of catchments in the western U.S. (Storck et al. 1998; Leung and Wigmosta, 1999; Bowling and Lettenmaier, 2001; LaMarche and Lettenmaier, 2001) and Canada (Nijssen et al., 1997; Wigmosta and Perkins, 2001; Whitaker et al., 2002; 2003).

2. APPROACH

The DHSVM sediment module predicts the range and variability of catchment sediment yield in response to dynamic meteorological and hydrologic conditions. DHSVM is a grid-based model (typically implemented at spatial resolutions from 30-150 m) that solves the energy and water balance for each grid cell for each time step. It was developed for mountainous watersheds overlain with shallow soils. The user-specified soil depths affect the dynamics of the subsurface moisture storage, vertical and lateral movement, and predicted saturation thickness. DHSVM determines runoff from saturation and infiltration excess – although the saturation excess mechanism, which is somewhat similar to that used in TopModel (Beven and Kirkby, 1979) is considerably more sophisticated than the infiltration excess mechanism, which is based on a static infiltration rate. Precipitation throughfall is determined based on the canopy coverage, and snow interception, melt, and drip from the overstory are also modeled. Forest road networks and their interception of subsurface flow and runoff are represented, and DHSVM determines flow through road-side ditches as well as through the stream channel network (Wigmosta and Perkins, 2001).

The DHSVM sediment module consists of four primary components: mass wasting, which is stochastic in nature; hillslope erosion; erosion from forest roads; and a channel-routing algorithm. DHSVM provides a continuous temporal sequence, spatially distributed over a watershed, of the following variables used in the sediment computations: depth to saturation, saturation and infiltration excess runoff, precipitation, leaf drip (assuming that all water that hits the canopy becomes leaf drip), and channel flow (Figure 1).

The sediment module follows the same conceptual foundation that has been used in stochastic slope-stability models (e.g., Hammond et al., 1992; Koler, 1998). The main difference is that slope failures are based on the dynamic simulation of soil saturation by DHSVM, from which time-varying pore pressure, and hence failure probabilities, are computed. The conceptual framework also draws from the SHETRAN/SHESED modeling system which incorporates mass failures and rule-based redistribution of sediment (Wicks and Bathurst, 1996; Burton and Bathurst, 1998). Major differences between the DHSVM sediment module and the SHETRAN/SHESED modeling system are the use of stochastic mass failure predictions and the representation of forest roads.

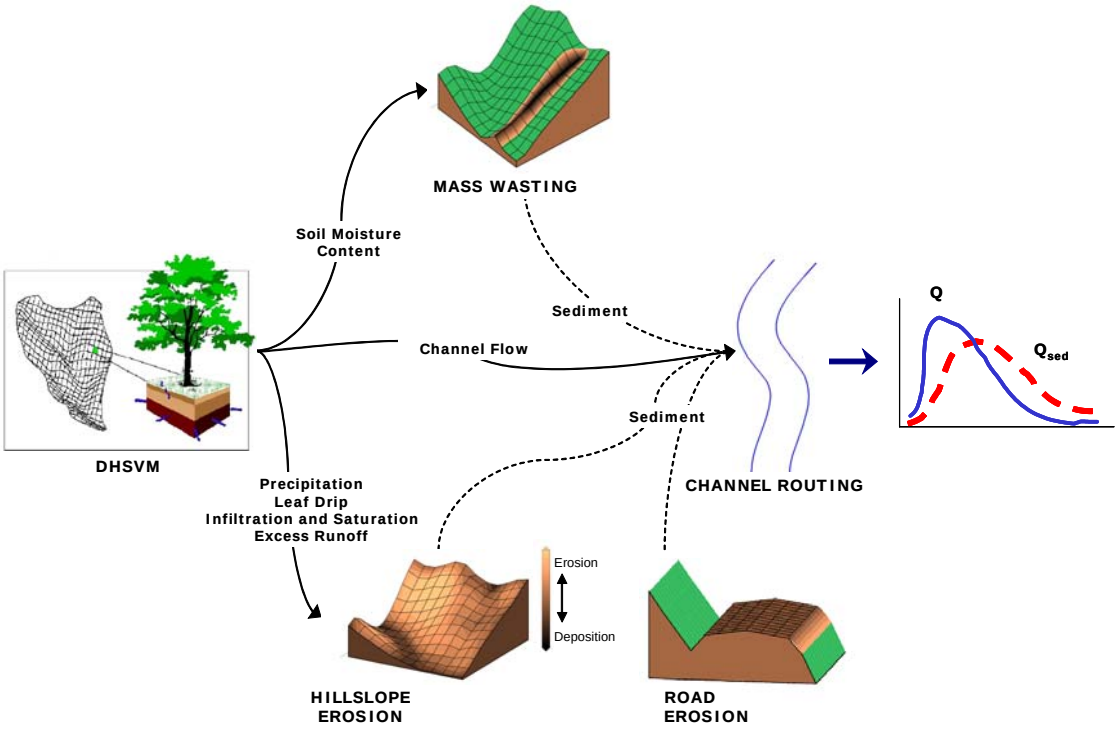

Figure 1. Sediment module schematic

3. DHSVM SEDIMENT MODULE DESCRIPTION

3.1. Mass Wasting

The mass wasting algorithm has two primary functions: failure prediction and downslope redistribution of material released from slope failures. This component is stochastic in nature and results in an event probability of failure.

3.1.1. Failure Prediction

Failure prediction is based on the concept that hydrological triggering of mass failures occurs when local pore pressure reduces shear strength below the imposed stresses. Soil saturation is determined within DHSVM using the subsurface routing scheme of Wigmosta and Lettenmaier (1999). To avoid excessive computation time, the mass wasting algorithm is only run for the single timestep during an event with the greatest basin saturation extent. An event is defined as a time period where saturation thresholds are met and is bracketed by two days, preceding and following, when those thresholds are not met.

The mass wasting algorithm calculations are partially performed at a finer spatial resolution than used by DHSVM for its hydrological computations. Soil moisture at the DHSVM resolution is redistributed to the fine resolution using the TOPMODEL topographic wetness index (Beven and Kirkby, 1979) and is calculated in the manner of Burton and Bathurst (1998) equation (7).

$$z_i^{'} - z^{'} = \frac{\left(I - I_i\right)}{f} \tag{1}$$

where $z_i^{'}$ is the potential soil moisture deficit in the fine grid cell, m; $z^{'}$ is the mean value of $z_i^{'}$ of all fine mesh grid cells in the DHSVM grid cell, m; I is the mean value of the topographic index over all fine grid mesh cells in the DHSVM grid cell; I_i is the topographic index for the fine grid cell, and is calculated according to Wolock and McCabe's (1995) method for multiple flow direction; and f is the constant that relates transmissivity to depth (required input for DHSVM). Because $z_i^{'}$ is a potential value, it is constrained by zero (no ponding is allowed) and the soil depth. The redistribution method does not ensure the conservation of mass (Burton and Bathurst, 1998), therefore initial computed values are used to compare the total soil moisture in the fine mesh grid cells within a coarse grid, to the volume in that coarse grid. Any deficit or excess water is redistributed using the ratio of I_i/I. This notation, as well as other notation used

throughout, is summarized in Appendix A.

Once the fine-resolution saturation deficit is determined, factor of safety computations begin and are performed on a cell-by-cell basis. Screening criteria are used throughout the algorithm to limit computations to critical areas. The first criterion ensures the fine mesh grid cell has sediment (i.e. it was not removed during previous failures, in either the current or previous time steps), and the saturation is greater than a fixed threshold. Second, the slope in the direction of steepest descent, calculated based on the sediment elevation of eight neighboring grid cells, must be greater than 10º. This limit was conservatively selected because reported values and slope stability theory indicate that shallow landslides are infrequent on slopes less than 25º (Sidle et al., 1985, Reneau and Dietrich, 1987; Burton and Bathurst, 1998). If these criteria are not met, the grid cell is assumed not to have failed, and the factor of safety computation is not performed.

If the above criteria are met, failure likelihood is determined using the well-known factor of safety (FS) analysis based on the infinite slope model (e.g., Ward et al., 1981; Selby, 1982; Burton and Bathurst, 1998; among others):

$$FS = \frac{\left(\frac{2(C_s + C_r)}{\gamma_w d \sin(2S)} + \frac{(L-m)\tan\phi}{\tan(S)} \right)}{L} \tag{2}$$

where :

$$L = \frac{q_0}{\gamma_w d} + m\frac{\gamma_{sat}}{\gamma_w} + (1-m)\frac{\gamma_m}{\gamma_w} \tag{3}$$

and C_s is the effective soil cohesion, kg/m^2; C_r is the root cohesion, kg/m^2; m is the relative saturated depth (dimensionless); ϕ is the effective angle of internal friction of soil on impermeable layer; γ_w is the weight density of water, kg/m^3; d is the soil depth above failure plane, m; S is the surface slope; q_0 is the vegetative surcharge per unit plan area, kg/m^2; γ_{sat} is the weight density of saturated soil, kg/m^3, and is determined from the average bulk density of all soil layers (required input for DHSVM); and γ_m is the weight density of soil at field moisture content, kg/m^3. Instability (grid cell failure) is indicated by FS values less than one. The algorithm generates stochastic results through the use of user-specified probability distributions (either normal, triangular, or uniform) for four of the parameters that define shear strength and loading: soil cohesion, angle of internal friction, root cohesion and vegetation surcharge. In our

implementation, the probability distributions and their parameters are based on published values (Table 1 and Appendix B). In some instances the randomly selected parameters may result in unconditional (not a function of soil moisture) instability. These pixels are not permitted to fail.

3.1.2. Mass Redistribution

The rule-based redistribution of failed material involves estimation of the failure volume, as well as the direction and distance of movement. Instead of imposing a landslide size, failures occur one grid cell at a time; and therefore, the minimum failure width is equal to the narrowest grid dimension. All the sediment on the failed grid cell is routed downslope, in the direction of steepest descent based on the bedrock slope. The failure calculations then proceed in this downslope direction. The slope associated with the downslope cell is recalculated accounting for the changes in sediment depth, and the FS is calculated with the new slope and soil loading. If this grid cell fails, the failure continues to propagate downslope. At any time the failure encounters a channel, the material enters the channel network. If a channel is not encountered, the failure ceases to propagate when a stable pixel is reached. Then the material runs out until a slope less than a fixed threshold (which we have taken as four degrees following Burton and Bathurst (1998)), is encountered. The wasted material is evenly distributed along the runout path of unfailed cells following Burton and Bathurst (1998). Material that enters the channel network can travel through the network as a debris flow. In DHSVM, the channel network is represented by a series of connected reaches (vectors) and each reach may span multiple grid cells. If the junction angle between reaches is less than 70º, movement continues as a debris torrent (Benda and Dunne, 1997). For junction angles greater than 70º, all transported sediment is divided equally between the upstream and downstream channel segments. Debris flows also stop and deposit all transported sediment if the channel segment slope (required input for DHSVM) falls below a fixed threshold, which we take as 3.5 degrees following Benda and Dunne (1997). Since failures are tracked down slope from the initial failed grid cell, if a failure has already occurred for a given pixel at the same time step (e.g., as a consequence of failure of an upslope cell) it is not allowed to fail again.

This process is repeated for multiple ensemble members, and every time a FS is calculated, new parameters are selected from the specified distributions. Therefore the same grid cell will have different parameters for each event and each ensemble member in that event. The changes in

sediment depth due to mass wasting and deposition are tracked for each ensemble member. After computations have been performed for all ensemble members for the current time step, the changes in sediment depth are averaged to create a sediment map (initially, the soil depth map required for DHSVM hydrologic computations) which is used as the initial condition for future time steps. In the interest of computational efficiency and because the changes in soil depth and topography are likely to have low impact on the hydrological predictions, the evolving sediment map is not utilized by the hydrology model (although in principle this could be done). Instead the hydrology calculations are based on the temporally constant soil depth map. The amount of sediment added to each channel segment, from debris flow routing, is also averaged over the ensemble members.

3.2. Surface Erosion

The surface erosion algorithm represents the mechanisms by which sediment is eroded from hillslopes and forest roads and transported to the stream or road-side ditch network. It is deterministic in nature, and therefore is unconnected to the failure scenarios predicted by the mass wasting algorithm. Surface erosion is computed at the DHSVM spatial resolution, rather than the higher resolution of the mass wasting algorithm. We assume that there is unlimited sediment available for detachment.

Runoff generation from each grid cell, including infiltration and saturation excess runoff, and culvert return flow is determined by DHSVM, as described by Wigmosta et al. (1994) and Wigmosta and Perkins (2001), with corrected inconsistencies in the runoff routing direction including checks to account for depressions/flat areas in the digital elevation model (DEM). Infiltration excess runoff is based on either a static (previously used by DHSVM), or dynamic (described below) maximum infiltration capacity. The Smith and Parlange (1978) method of calculating a dynamic maximum infiltration capacity threshold as a function of water infiltrated is used in the DHSVM sediment module, in the manner of KINEROS (Smith et al., 1995), where:

$$f_c = K_s \frac{\exp(Inf / B)}{\exp(Inf / B) - 1} \tag{4}$$

is the infiltration rate after ponding, m/s, and

$$B = (G + h)*(\theta_s - \theta_i) \tag{5}$$

in which K_s is the hydraulic conductivity, m/s; Inf is the cumulative amount of infiltrated water

since ponding started, m; G is the mean capillary drive, m; h is the surface water depth, m; θ_s is the effective saturation, approximated as the porosity (required input for DHSVM), fraction; and θ_i is the fractional soil moisture content when ponding first started.

Runoff generation is partitioned, based on the area of the road in the grid cell, for routing over the hillslope and over the road surface. For both surfaces, overland flow is modeled using an explicit finite difference solution of the kinematic wave approximation to the Saint-Venant equations (Chow et al., 1988):

$$\frac{\delta Q}{\delta x} + \frac{\delta A}{\delta t} = i(x,t) \tag{6}$$

where Q is inflow of water, m^3/s; A is cross-sectional area of flowing water, m^2; and i is saturation and infiltration excess, $m^3/s/m$. The solution time step, Δt, is dynamically calculated according to the Courant condition to maintain solution stability while minimizing run time.

The algorithm uses methods for surface erosion prediction similar to the mechanistic models EUROSEM (Morgan et al., 1998), SHESED (Wicks and Bathhurst, 1996) and KINEROS (Woolhiser et al., 1990). Sediment available for transport is routed using a four-point finite difference solution of the two-dimensional conservation of mass equation such that total erosion is limited by transport capacity (Wicks and Bathurst, 1996):

$$\frac{\delta (QC)}{\delta x} + \frac{\delta (AC)}{\delta t} = e(x,t) \tag{7}$$

where C is the current local sediment concentration, m^3 sediment/m^3 water, and e is the net erosion, m^2/s.

3.2.1. Hillslope Erosion

Hillslope sediment supply is calculated based on detachment energy of raindrops, leaf drip, and overland flow. Raindrop detachment is calculated according to Wicks and Bathhurst (1996) and is proportional to the fraction of vegetative cover (both understory and overstory), the momentum of throughfall and leaf drip and an empirical soil erodibility coefficient. It also accounts for reduced detachment with increasing runoff depth.

Water and sediment routing calculations proceed from the highest grid cell to the lowest. Overland flow is routed prior to implementation of the erosion algorithm, so the depth and velocity of flow are available for sediment calculations. Sediment transport is calculated using a

modified version of the finite difference equations used by the SHETRAN/SHESED model (Wicks and Bathurst, 1996).

$$C_i^t = \frac{\left\{ C_{i-1}^t \left[\frac{\theta}{\Delta x} Q_{i-1}^t - \frac{\alpha}{2\Delta t} Q_{i-1}^{t\beta} \right] + C_i^{t-1} \left[\frac{\alpha}{2\Delta t} Q_i^{(t-1)\beta} - \frac{1-\theta}{\Delta x} Q_i^{t-1} \right] + C_{i-1}^{t-1} \left[\frac{\alpha}{2\Delta t} Q_{i-1}^{(t-1)\beta} + \frac{1-\theta}{\Delta x} Q_{i-1}^{t-1} \right] + D_r + D_{of} \right\}}{\left[\frac{\alpha}{2\Delta t} Q_i^{t\beta} + \frac{\theta}{\Delta x} Q_i^t + \beta_{de} \Delta y v_s \right]} \quad (8)$$

where the Q is runoff, m^3/s, and Δx and Δy are the grid cell dimensions, m. The left side of this equation is the sediment outflow concentration from the cell, m^3/m^3, for the current sub-time step; the first three terms on the right side are the inflow concentration from the upslope grid cell at the current sub-time step, and the outflow concentration from the previous sub-time step from the current grid cell and upslope grid cell, respectively. A was defined in terms of Q using Manning's equation, resulting in: $\alpha = n * \Delta x^{2/3} / S^{1/2}$ and $\beta = 2/3$. The time weighting factor, θ, is initially set to 0.55. The last two terms on the right side are D_r, soil detached by raindrop impact, $m^3/s/m$ and $D_{of,}$ soil detachment from overland flow, $m^3/s/m$, which is equal to $\beta_{de} \Delta y v_s TC$, where β_{de} represents detachment efficiency. v_s is the settling velocity, m/s, and TC is the transport capacity, m^3 sediment/m^3 water. Particle detachment is known to be related to soil cohesion, among other things (Morgan et al., 1998). Since a physical representation is yet to be formulated, we approached this in a manner similar to Morgan et al. (1998). We determine β_{de} from soil cohesion, but in a slightly different manner:

$\beta_{de} = 0.79e^{-0.6Cs}$

where cohesion is in kPa. TC is determined according to the method of KINEROS2:

$$TC = \frac{0.05}{d_{50}(\gamma_w - 1)^2} \sqrt{\frac{Sh}{g}} (\Omega - \Omega_c) \quad (9)$$

where:

$$\Omega = uS \qquad \text{m/s} \quad (10)$$

and u is the flow velocity, m/s, calculated from the surface routing; d_{50} is the median particle diameter, m; g is acceleration due to gravity, m/s^2; and Ω_c is the critical value of 0.004 m/s used in KINEROS2. This assumes that outflow is a power function of unit storage, as did Smith et al. (1995), Morgan et al. (1998) and Ziegler et al. (2001). In our application, the transport capacity of flow with depths less than 0.001 m is assumed to be zero, since tests using TC < 0.4, based on maximum concentrations reported in Govers (1992), indicate this is a critical value. The particle

settling velocity is calculated as in KINEROS (Smith et al., 1995):

$$v_s = \left(\frac{4}{3} g(SG - 1) \frac{d_{50}}{C_d} \right)^{0.5} \quad (11)$$

where:

$$C_d = \frac{24}{R_n} + \frac{3}{(R_n)^{0.5}} + 0.34 \quad (12)$$

is the drag coefficient,

$$R_n = v_s h / v \quad (13)$$

is Reynold's number, and v is the kinematic viscosity, m^2/s, and is determined based on dew point temperature; and SG is the specific gravity. Equation (8) provides the sediment concentration from overland flow. If the flow is unable to carry the calculated outflow, deposition will occur. The mass of outflow for the current sub-time step is accumulated for each sub-time step (as determined by the Courant Condition), up to the DHSVM time step. To limit computational time, the hillslope surface erosion algorithm can be run for a specified time period(s).

3.2.2. Forest Road Erosion

By construct, in DHSVM road surface flow does not travel from cell to cell but enters the road-side ditch in the grid cell in which it was generated (Wigmosta and Perkins, 2001). This convention remains unchanged, although routing now accounts for road crown type. Water is routed across the road to the road-side ditch, and/or to the hillslope depending on whether the road is crowned, insloped or outsloped.

For the finite difference solution of the kinematic wave equation, the road surface area is discretized into square grid cells in the following manner. The slope of the road in the direction of flow is:

$S_{flow} = sqrt(S_{crown}^2 + S_{road}^2)$

The length in direction of flow is determined based on the above calculated slope as:

$L_{flow} = W_r * (S_{flow}/S_{crown}) * sqrt(1 + S_{crown}^2)$.

where W_r is the road width, m. If the road is crowned, half of the flow length is used. This length is divided by a user-specified factor to determine the cell length and number of computational cells. Cells are assumed to be oriented in the direction of flow. Since grid cells are square, the cell area is determined from the cell length and the number of grid cells is calculated as *road*

area/cell area. The road characteristics are uniform for the road segment in the grid cell, therefore the routing calculations are performed for a single column of cells. Routing across the road surface proceeds from the highest point (the crown or edge of an outsloped or insloped road) to the road-side ditch or hillslope. The calculated outflow is multiplied by the number of cells in a row prior to discharging.

Forest road erosion is modeled similarly to the hillslope erosion and in the manner of KINEROS (Woolhiser et al., 1990; Ziegler et al., 2001). Total erosion is calculated based on raindrop impact and overland flow detachment. Soil particle detachment by raindrop impact is calculated based on the rainfall intensity and an empirical soil erodibility coefficient. It also accounts for reduced detachment with increasing runoff depth. Soil particle detachment by overland flow, $m^3/s/m$, is calculated as:

$$D_{of} = c_g(TC - C)A \tag{14}$$

where:

$$c_g = CHv_s/h \tag{15}$$

is the transfer rate coefficient, 1/s, and CH is an erodibility coefficient. Transport capacity is calculated using the same method as for hillslope erosion except that Ω_c is set at 0.0004 m/s and for flow depths less than the d_{50}, TC is zero. When equation (7) is solved for road surface erosion, the result is the same as equation (8) with the following replacement: $c_g \alpha Q^{\beta} = \beta_{de} \Delta y v_s$

Sediment is also routed according to the crown slope: i.e. if the road is crowned or insloped, sediment is added to the road-side ditch, and if the road is outsloped or crowned sediment is routed to the hillslope. Sediment from the road surface and hillslope are available for transport through the road-side ditch network. All road-side ditch segments have a culvert and all sediment that is routed to the culvert is discharged through the culvert. If the culvert is in a grid cell with the stream channel, the percent of the sediment discharged to the stream channel is a function of the particle size (Table 2) which is a conservative approach based on the work by Duncan et al. (1987). Section 3.3 describes the particle size distribution in the road-side ditch network. Otherwise, all sediment is discharged to the hillslope.

3.3. Channel Routing

Sediment enters the stream and road-side ditch network as the result of debris flows originating from mass wasting or as lateral inflow from hillslopes or forest roads. All debris

flows entering the channel have a fixed lognormally distributed grain size distribution (Sturm, 2001). The d_{50} and d_{90} size particles of the distribution are user-specified as is the number of sediment size classes, which are tracked independently. The sediment is distributed into the defined number of sediment classes according to the lognormal distribution, with the representative diameter for each class set at the median particle size for that class. Sediment from the hillslope and the road surfaces is added to the appropriate classes based on their user-specified d_{50}. The debris inflow is computed on a volumetric basis, which is converted to a mass using the Komura (1961) relationship for density of a sediment mixture.

Channel discharge is computed by DHSVM for each channel segment using a linear reservoir routing scheme. It incorporates lateral inflow via both overland flow and intercepted subsurface flow (Wigmosta et al., 1994 and Wigmosta and Perkins, 2001). Sediment inflow to each channel segment at each time step consists of the sediment entering from the upstream reach(es), and the sediment added to the stream reach locally. Local contributions of sediment to a stream reach are assumed to be uniformly distributed along the reach.

The channel sediment routing is based on Wicks and Bathurst (1996), beginning with a mass balance (similar to their Equation 12). When written in terms of mass this produces the well-known Exner equation (Exner, 1925):

$$\frac{\partial}{\partial t} AC\rho_s + \frac{\partial}{\partial t} m_S + \frac{\partial}{\partial x} ACV\rho_s = \rho_s q_s \tag{16}$$

where m_s is the mass of sediment stored in the bed per meter of channel length, kg/m, and is equal to $W_c z \rho_s (1-\lambda)$; W_c is the channel width, m; z is the bed sediment depth, m; ρ_s is the sediment particle density, kg/m^3; λ is the bed porosity; V is the average channel flow velocity, m/s; and q_s is the local volumetric sediment inflow rate to the reach per meter of channel length, m^3/s/m. Note that Wicks and Bathurst (1996) use sediment velocity rather than V as shown above, however based on a mass balance V (mean fluid velocity) was used instead of the sediment velocity.

Where changes in the suspended sediment storage are small compared to the changes in bed material storage, the first term in equation (16) is negligible and the above equation can be simplified to:

$$\frac{\partial}{\partial t} m_S + \frac{\partial}{\partial x} AcV\rho_s = \rho_s q_s \tag{17}$$

This equation is solved across a channel segment in the following manner. Similar to the surface

erosion component, the solution time step is dynamically calculated according to the Courant condition, by setting $V\Delta t/\Delta x$ to approximately one, to maintain solution stability while minimizing run time. Since the DHSVM channel hydraulic calculations precede the sediment routing, the instantaneous upstream and downstream flow rates at each sub-time-step are estimated based on the rate of change inflow and outflow rates. Total sediment transport capacity, in immersed weight per meter of channel width, for both the upstream and downstream flow rates is calculated using Bagnold's equation (Bagnold, 1966; Graf, 1971):

$$TC_c = \omega\left[\frac{e_b}{\tan\alpha} + 0.01\frac{V}{V_{ss}}\right] \tag{18}$$

where e_b is a function of the mean flow velocity and is estimated by empirical relationships; $\tan\alpha$ is a function of the dimensionless bed shear stress and is also estimated by empirical equations; and V_{ss} is the settling velocity, m/s, calculated using Rubey's (1933) equation, and

$$\omega = \rho g D S_c V \tag{19}$$

is the stream power per unit bed area, J/s/m^2, where ρ is the density of water; D is the flow depth, m, solved using outflow from DHSVM and Manning's equation; and S_c is the energy gradient (assumed equal to the channel slope). The calculated TC_c is limited to d > 0.015 mm (Graf, 1971). Particles of this size are considered part of the wash load (d <= 0.062 mm) and are always transportable.

Changes in bed material storage are estimated using the finite difference equation from Wicks and Bathurst (1996):

$$\frac{\partial}{\partial t} m_s \approx \varphi\left(Q_s W_c\right)_i + \left(1-\varphi\right)\left(Q_s W_c\right)_{i-1} \tag{20}$$

where φ is a space weighting factor (initially set to 0.55) and

$$Q_s = \frac{TC_c}{g\left(1-\frac{\rho}{\rho_s}\right)} \tag{21}$$

is the transport capacity in dry mass per unit width, kg/m/s. If m_s exceeds the available sediment on the bed, it is reduced to the available sediment divided by the sub-time-step length. The Exner equation is solved for downstream sediment outflow rate for the channel reach for the current time step:

$$C_i^t = \frac{1}{\theta}\left[\theta\left(ACV\rho_s\right)_{i-1}^{t+1} - (1-\theta)\left(\left(ACV\rho_s\right)_i^{t-1} - \left(ACV\rho_s\right)_{i-1}^{t-1}\right) + \rho_s q_s \Delta x - \frac{\partial}{\partial t} m_s\right] \Big/ \left(AV\rho_s\right)_i^t \quad (22)$$

where Δx is the stream segment length; the left side of this equation is the sediment outflow concentration from the reach, m^3/m^3, for the current sub-time step; the first three terms on the right side are the inflow rate, kg/s, to the reach at the current sub-time step, and the outflow and inflow from the previous sub-time step, respectively; the last two terms on the right side are the lateral sediment inflow rate in and the change in mass storage, as calculated in previous steps; and θ, the time weighting factor, initially set to 0.55, is dynamically adjusted for calculation stability. When there are large lateral inflows due to mass wasting contributions or when $C_{t-1} >> C_t$ or vice versa, θ is set to 1. If the outflow rate exceeds the transport capacity, it is set to the transport capacity and the difference in sediment mass is added back to the sediment mass in storage in the channel bed. Routing is performed for each particle size class starting with the smallest class. As transport capacity is used, it is not available for the remaining particle sizes. The mass of outflow for the current sub-time step is accumulated for each sub-time step, up to the DHSVM time step.

Table 1. Sediment module parameters

Parameter	Use	Range of values	Sources
Soil			
Manning's roughness coefficient, n	hillslope runoff routing	0.01 – 0.02	KINEROS2 model documentation, which references Engman (1986) and Woolhiser (1975)
Kindex	hillslope erosion	30 – 62 1/Joule	Wicks and Bathurst (1996)
d_{50}	hillslope erosion	0.1 – 20. mm	Dietrich et al.(1982)
soil cohesion distribution	factor of safety calculation	4.5 – 22 kPa	Hammond et al. (1992) and others
effective angle of internal friction distribution	factor of safety calculation	29 – 42 degrees	Hammond et al. (1992)
Vegetation			
root cohesion distribution	factor of safety calculation	2.0 – 23. 0 kPa	Hammond et al. (1992), Burroughs and Thomas (1977), Montgomery et al. (1998), Dietrich et al. (1995), Wu et al. (1979), Wu (1984), Ziemer (1981)
vegetation surcharge distribution	factor of safety calculation	0 – 195.4 kg/m^2	Hammond et al. (1992)
Roads			
Manning's roughness coefficient, n	runoff routing	0.015 – 0.02	KINEROS2 model documentation, which references Engman (1986) and Woolhiser (1975).
erodibility coefficients	road surface erosion	Rainsplash: 200 – 300 Overland flow (CH): 0025 - 0.35	Smith et al. (1999)
d_{50}	road surface erosion	0.1 – 10 mm	Dietrich et al.(1982)

NOTE: See Appendix B for all values used

Table 2. Sediment delivery from culverts to streams

Particle size (mm)	Percent Delivered
0.5 – 2	10
0.063 - 0.5	30
≤ 0.063	100

4. IMPLEMENTATION AND TESTING

The DHSVM sediment module was tested in the Rainy Creek tributary of the Little Wenatchee River basin which drains the eastern slope of the Cascade Mountains (Figure 2) in north central Washington State. It has a drainage area of approximately 44 km^2 and eventually discharges to the Columbia River via the Wenatchee River. It is a snowmelt-dominated catchment with inferred mean annual precipitation ranging from 230 cm at higher elevations to 150 cm in the lower elevations according to Parameter-elevation Regressions on Independent Slope Model (PRISM) maps of annual mean precipitation (Daly et al., 1994; Daly et al., 1997).

Because the DHSVM sediment module was developed for the purpose of evaluating effects of alternative land management scenarios and forest disturbance, we evaluate its performance with respect to the effects of forest roads and fire on sediment generation in the Rainy Creek basin. Specifically, we test scenarios that include the existing road network, a partially decommissioned network, and no roads, all with current (2001) vegetation data. We also test a scenario with a simplistic representation of a catchment-wide fire.

4.1. Spatial characteristics data

Spatial characteristics are parameters that vary grid cell by grid cell but do not change over the simulation period. They include parameters related to topography (elevation, slope, aspect) and a number of soil and vegetation characteristics. These data were provided by the United States Department of Agriculture (USDA) Forest Service Pacific Northwest Research Station (PNRS) and Wenatchee Forestry Sciences Laboratory (WFSL). The basin is represented by 49,085 grid cells at 30-meter spatial resolution. The DEM was preprocessed in a manner similar to Tarboton et al. (1991) to fill sinks in four directions and to force flat areas to have a drainage direction. According to the DEM, the basin ranges in elevation from 630 m to 2150 m. Slopes range from 0 to 66 degrees with a mean of 26 degrees.

Eight soil types are present in the basin, with over eighty percent of the basin being sandy or fine sandy loam (Figure 3). The remainder of the basin soils consists of loamy sand (3%), loam (2%) and rock (9%). The soil depth map was created by the PNRS and WFSL as described in Appendix C. In some areas it included soils in excess of 9 meters in depth. Typical failures in the PNW occur below the root zone at depths from 0.2 to 2 m (Schmidt et al., 2001). Since the

factor of safety calculation requires the depth of soil above the failure plane and we use the total soil depth from the soil depth map, the soil depth was truncated at 2 m to be representative of rooting depths (Figure 3). Vegetation in the basin consists of ponderosa pine, grand fir, white fir, Pacific silver fir, western larch spruce or subalpine fir, western hemlock, western red cedar, Douglas-fir, western white pine, sugar pine, lodgepole pine, Engelmann spruce, mountain hemlock and whitebark pine. Twenty-one vegetation classes were defined with many of the vegetation types differing only by fractional cover over the grid cell and overstory height (Figure 3 and Appendix D).

The stream network was created from the DEM in ArcInfo assuming a support area of four hectares (ha). Although we do not have direct observations of the support area, Storck et al. (1998) observed a support area in two small western Cascade catchments of approximately two ha, and Rainy Creek is on the drier, east slopes of the Cascades where support areas are expected to be larger. Furthermore, a support area of greater than nine ha is needed to create the blue lines on the US Geological Survey maps for Labyrinth Mountain and Mount Howard (1:24,000 series) and it is known that blue lines are often inadequate in representing the actual network extent (Montgomery et al., 1998). The stream and road network files were processed using methods described in Bowling and Lettenmaier (1997). Total road length in the basin is 46 km and the road density is 1.05 km/km^2. The road network was divided at low points as well as divide locations, using the method of Wigmosta and Perkins (2001), resulting in 332 segments. All road and stream intersections (91) were assumed to be culverted as were low points in the road network (193) as determined by overlaying the road network on the DEM. Stream and road-side ditch width, depth and Manning's roughness coefficient were assigned based on classes adopted from Storck and Lettenmaier (2000) or information provided by PNRS and WFSL. Table 3 provides the road characteristics. Although infiltration through the road surface is allowed in the overland flow model, we set this parameter to zero to provide an upper bound on erosion of road surfaces.

4.2. Temporally varying data

The required DHSVM model forcings (precipitation, temperature, and windspeed) were taken from the nearest 1/8 degree grid cell (latitude 47. 8125, longitude -121.0625, elevation 1286.86 m) in the continental dataset of Maurer et al. (2002). Precipitation and temperature in this dataset

were interpolated from station observations, and daily windspeed was obtained from the NCEP/NCAR Reanalysis (Kalnay et al., 1996). The remaining required forcings (relative humidity, shortwave radiation and longwave radiation) were derived from precipitation and temperature as described by Maurer et al. (2002). This single time series was then adjusted to each of the DHSVM grid cells by lapsing temperature at -0.006 C/m and precipitation at 0.0007 m/m relative to a reference elevation. The model was run at a three-hour time step using forcing and spatial characteristics data as described above, and with other model parameters and constants taken from past model applications described by Storck et al. (1995), Bowling and Lettenmaier(2001), and LaMarche and Lettenmaier (2001).

4.3. Hydrology Results

DHSVM was initially run from 10/01/1991 to 9/30/1995. Because Rainy Creek is an ungauged river, results were evaluated by comparing the predicted hydrographs to those observed for other, larger tributaries of the Wenatchee River: Chiwawa River (data from water years 1992-1997) and Icicle Creek (data from water years 1994-1997). The simulated streamflows were compared to gauge flows scaled by basin area (Figure 4 and Table 4). According to average annual precipitation as determined using the PRISM maps (Daly et al., 1994; Daly et al., 1997), Rainy Creek receives more precipitation than the Chiwawa River and Icicle Creek basins. Therefore, the simulated hydrographs were judged to be reasonable. In addition, modeled snow water equivalent (SWE) was compared to observations at three stations (Table 5 and Figure 5). These show a slight delay in modeled relative to observed snow melt.

A second DHSVM run was performed for the independent period 10/1/1995 to 9/30/1997 and similar comparisons were made. The streamflow hydrographs showed similar results. A large rain-on-snow event occurred in November 1995 that resulted in flood events throughout the Northern Cascades. This is evidence by the decrease in SWE at the three SNOTEL stations accompanied by an increased flow at gauges on Chiwawa River and Icicle Creek. For Rainy Creek, no decrease in SWE or large streamflow response was predicted. Failure to reproduce this event indicates that the lapsed temperature based on the Maurer et al (2002) data was too cold. Since the focus of this work is the development and implementation of the sediment module, and for the remainder of the simulation period the simulated spring snowmelt was determined to be the peak time for surface runoff and basin saturation, the temperature inputs were not adjusted,

although such a temperature adjustment would undoubtedly increase runoff in the 1995 event considerably.

4.4. Model Sensitivity to Infiltration

The model was also run using dynamically determined maximum infiltration so that total infiltration and infiltration excess runoff could be compared. This required an additional soil parameter, capillary drive, which was selected based on values in KINEROS2 model documentation. For the six-year run, there was a maximum difference in the average daily basin-wide average runoff depth of less than 0.4 mm. Therefore, this option was not used in the remainder of the runs.

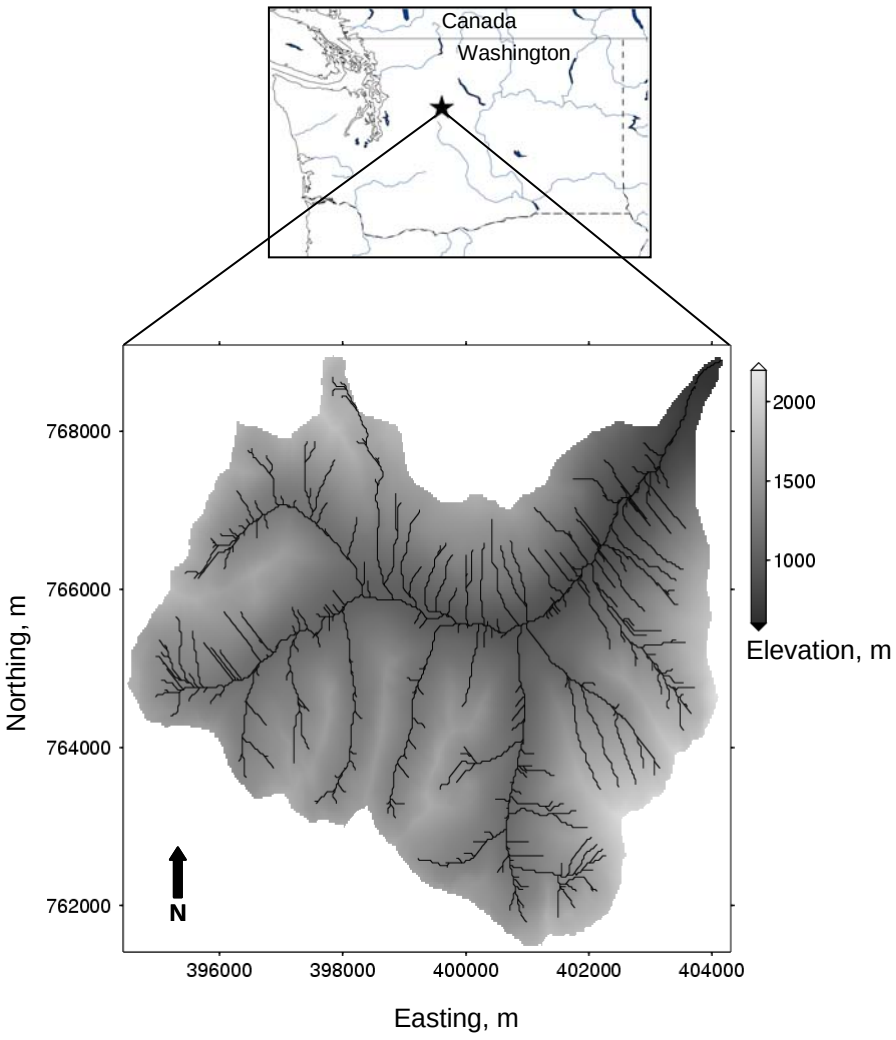

Figure 2. Rainy Creek basin site map

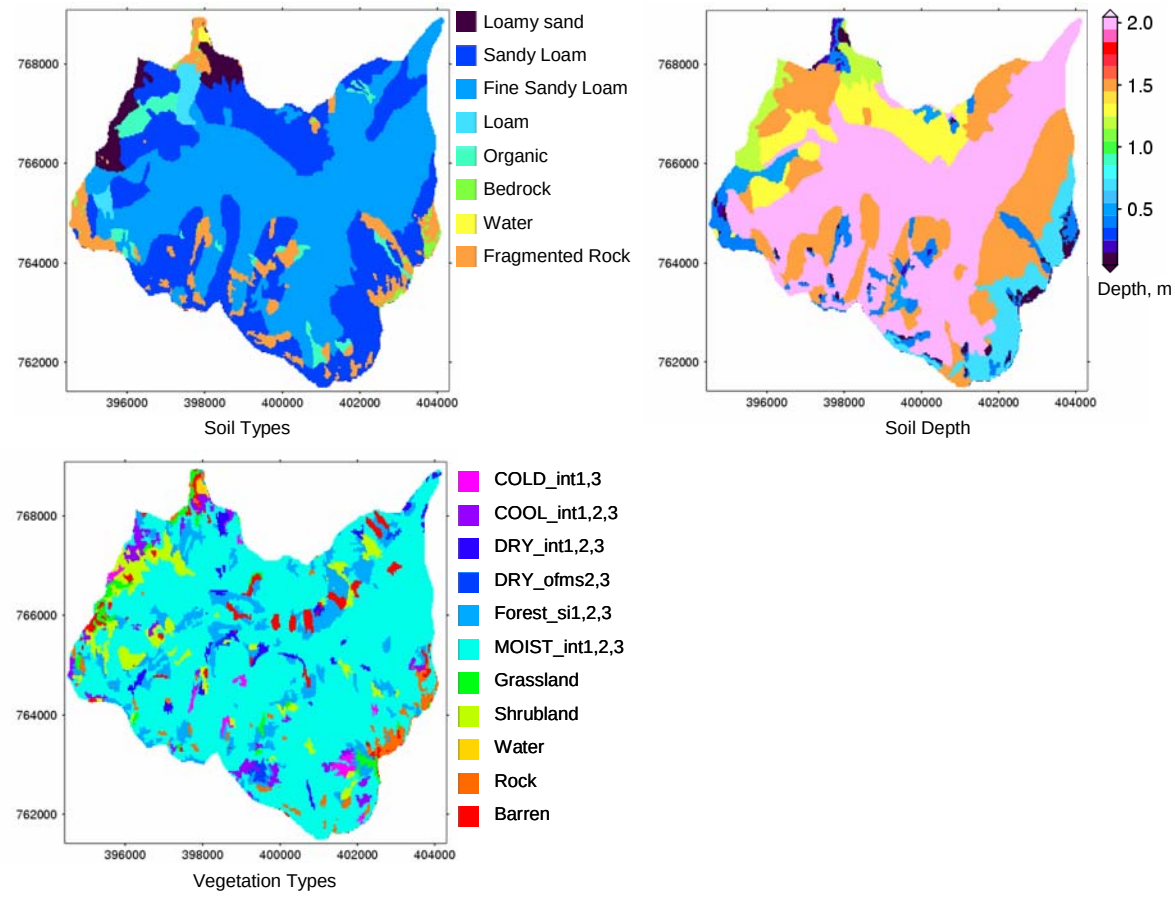

Figure 3. Rainy Creek soil and vegetation input maps

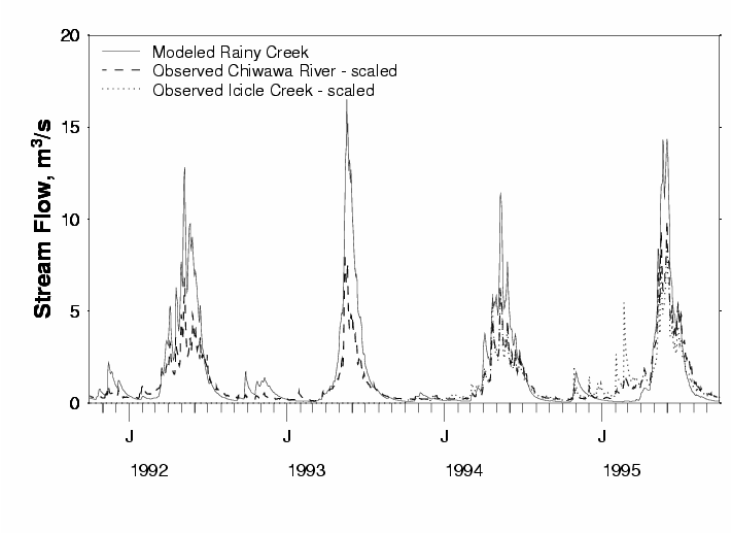

Figure 4. Modeled and observed streamflow. Observed Icicle Creek data begin on October 1, 1994.

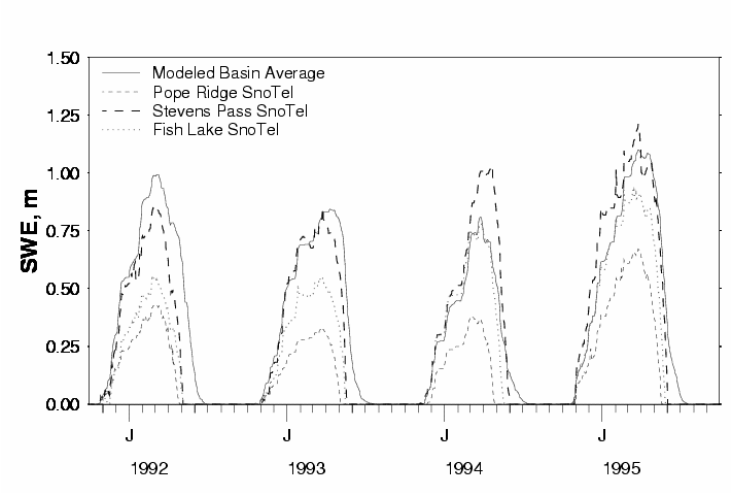

Figure 5. Modeled and observed snow water equivalent

Table 3. Road characteristics

Class ID	Description	Road Width, m	Crown Type	Ditch Width, m	Ditch Depth, m
106	Road, Unimproved, Class 4	4.267	Outsloped	0.914	0.305
515	Road, Light-Duty, Dirt, Class 3C	4.572	Insloped	0.914	0.305
518	Road, Light-Duty, Gravel, Class 3B	5.486	Crowned	1.219	0.305

Table 4. Stream gauges utilized during DHSVM calibration

Stream	USGS Gauge Number	Latitude	Longitude	Elevation, m	Basin Area, km^2	Average Annual Flow, m
Rainy Creek	N/A	N/A	N/A	N/A	44	N/A
Chiwawa River	12456500	47º50’15”	120º39’40”	640	440.3	1.15
Icicle Creek	12458000	47º32’38”	120º43’08”	442	499.7	1.06

Table 5. SNOTEL stations utilized during DHSVM calibration

Station	Station Number	Latitude	Longitude	Elevation, m	Average Annual Precipitation, m
Fish Lake	21b04s	47º31’	121º4’	1027	1.71
Pope Ridge	20b24s	47º59’	120º34’	1078	0.92
Stevens Pass	21b01s	47º44’	121º5’	1240	2.50

5. SEDIMENT MODULE IMPLEMENTATION

In addition to the input required for the DHSVM hydrology model, the sediment module requires a finer resolution DEM, additional soil and vegetation parameters, and additional road input parameters. The finer resolution DEM determines the minimum width of predicted failures. Sixty-one landslides inventoried in the central California Coast Ranges had widths that clustered around 7 to10 meters (Reneau and Dietrich, 1987), and a summary of reported shallow landslides, including the Reneau and Dietrich (1987) inventory, showed widths of 2.7 to 40 m (Burton et al., 1998). Therefore, a 10-meter DEM, provided by the USDA Forest Service, was utilized for the mass wasting prediction. Constant soil parameters required are the debris flow d_{50} (set to 2 mm) and d_{90}, particle sizes, (set to 17 mm). These values were used to represent the range of particles moved during mass wasting events. The road crown slope was set at 0.02 meters/meter. The required spatially variable parameters are shown in Table 1. The module was run for a six year period, from 10/1/1991 to 9/30/1997, for the existing conditions and road network. Parameters were adjusted during implementation to provide results closer to published rates. The results of each component are discussed below. In general, the results were used to calculate erosion rates. Since site-specific data are not available, these rates were compared to either published rates for various locations or estimated rates for Rainy Creek. Rates from other basins will differ from Rainy Creek due to climatic, lithologic and land use differences as well as due to the methodology used for deriving them (i.e. aerial photograph survey, plot studies, sediment budget estimates) and time period over which they were estimated.

5.1. Mass Wasting

Landslide rates and volumes for Rainy Creek were compiled from an aerial photograph survey (Bergen et al. 2003) using five stereo pairs spanning twenty-two years (1970-1992). Potential slides that were in the vegetation classes of “fragmented rock”, “bedrock” or “water” (as designated by the USDA Forest Service vegetation map) were not included. Slides were mapped with a high, medium or low confidence level to create a series of results. A description of this mapping methodology is provided in Appendix E. Slides designated as new were visible in one aerial photograph set and not in the preceding one (Table 6). All mapped slides were imported to ArcInfo and overlain on the soil depth map to estimate failed areas and volumes and failure rates.

An average failure rate between 1970-1992 for Rainy Creek of 3,035 kg/ha/yr was determined.

For the modeled time period, six potential mass wasting events, on 05/08/1992, 05/18/1993, 05/30/1995, 06/08/1996, 05/17/1997, and 06/15/1997, were identified based on saturation screening thresholds (at least 20% of the basin had a relative saturated depth of at least 0.85) (Figure 6). During implementation, sensitivity analysis showed the infinite slope model behaved as described by others (Gray and Megahan, 1981; Hammond et al. 1992, Wu and Sidle, 1995; Borga et al., 2002). The model was most sensitive to soil cohesion, root cohesion and soil depth, less sensitive to angle of internal friction and insensitive to saturated density and vegetation surcharge. Beyond truncating the soil depth at two meters (see Section 4.1), inputs to the DHSVM hydrology model (weight density of saturated soil, slope and soil depth), or variables calculated by the model (relative saturated depth) were not adjusted. Therefore, only soil cohesion, root cohesion and friction angle distributions were adjusted to fine tune results. Landslide probabilities were simulated for Rainy Creek by calculating the factor of safety for 100 iterations for each of the six events. The cumulative change in sediment depth over the modeled period was calculated by summing over all events the weighted average of sediment change over all iterations for each event. Figure 7a shows the cumulative change in sediment depth, which ranged from -0.7 m (failures) to 1.4 m (runout deposition), for the modeled period. The failure probability map (Figure 8) shows the maximum single event probability of failure, which ranged from 0 to 28 percent, for the modeled period. Areas that had a probability of failure greater than zero had the following characteristics: 81.9% had soil depth greater than 1.5 m (11.8% of areas with soil depth greater than 1.5 m), 25.8% had soil type of loam or organic (modeled with the same parameter distributions as loam) (40.0% of areas with these soil types) and 40.4% had a vegetation type of shrubland or barren (38.5% of areas with these vegetation types). The mean slope of areas that failed was 30.7 degrees.

A simulated landslide rate of ~5,700 kg/ha/year was determined as an average over the simulation period. This is greater (by a factor of about two) than the rate determined from the aerial photograph survey based on all slides (sixty-two) that were mapped. However, aerial photograph mapping tends to underestimate the number of slides and landsliding rate, due to obscuring by vegetation overstory and large time gaps between photographs allowing for slides to occur after one photograph and become undetectable before the next photograph. On the other hand, rates compiled from eight Pacific Coast studies, spanning 6 to 84 years, suggest the

predicted rate may be too high (Amaranthus et al., 1985). Simulated failures occurred in topographic hollows, similar to those mapped, as well as on steep side slopes, with deposition on the hillslopes and sediment delivery to the channel network. While failures on steep sideslopes do occur, the extent simulated in two areas was surprising because these areas typically are more stable than topographic hollows, where deeper soils and subsurface flow accumulate and root cohesion may not provide enough stability during large storms (Reneau and Dietrich, 1987). However, a large part of these sideslopes were either unvegetated (vegetation class barren) or had vegetation with lower root cohesion, relative to the rest of the basin, (vegetation class shrubland). These classes exist on deeper soils (< 1.5 m) and steeper slopes (> 35 degrees). While only 7.4 percent of the failed areas have these characteristics, they contribute ~1,250 kg/ha/year to the calculated rate. Discounting those areas with prescribed soil depths that seem unrealistically large, the annual failure rate of 4,450 kg/ha (0.26 mm/yr) is much closer to the rate determined from the aerial photograph survey. Another basis for comparison is the long-term erosion rate of 0.02 – 0.15 mm/yr determined for the area south of Rainy Creek in the eastern Cascades by Reiners et al. (2003). However, based on elevation and inferred precipitation for Rainy Creek, the long-term erosion rate may be argued to be somewhat higher than that estimated by Reiners et al, perhaps in the 0.1-0.2 mm/yr range. In any event, the simulated rate is greater than the background rate and may indicate that anthropogenic influences (harvesting) are increasing erosion rates.

The mapped slide locations (including slides in all confidence levels) and simulated failure areas do not correlate well (Figure 7a). The slides were mapped over a twenty-two year period that included harvesting activities in the 1970s and 1980s. Comparison of mapped slides to a time series of peaks over threshold (POT), with a threshold value of ~0.4 cubic meters per second based on a gauge for the Wenatchee River at Peshastin (USGS No. 1245900 and nearest gauge with a complete record for this time period), showed that higher flows in the 1970s did not correlate with higher slide rates. This suggests that anthropogenic influences were more substantial than meteorological. Because our model runs utilize a temporally constant vegetation map based on April 2000 conditions that likely differs from the historic vegetation coverages, the landslide locations may understandably differ. When the mapped slides are overlain on a map with vegetation age (based on height and vegetation class description (Appendix D)) , approximately half (52%) of the mapped slides occurred in vegetation category two (Figure 7b).

The majority of simulated failures, ~4,300 kg/ha/yr, occurred in vegetation category one, the youngest category. This suggest that simulated and actual failures are more likely in younger vegetation and due to differences in simulated and historic vegetation coverages, failure locations do not match.

5.2. Surface Erosion

In an effort to reduce computation time, the hillslope erosion component was run for time periods of maximum runoff (05/05 - 5/12/1992; 05/18 - 05/31/1993; 05/08 - 05/15/1994; 05/21 - 06/06/1995; 06/04 - 06/18/1996; 05/16 - 05/21/1997; 06/14 - 06/20/1997; 07/06 - 07/12/1997). During model runs, the formula of the particle detachment efficiency, β_{de}, was adjusted until the formulation specified in Section 3.2.1 was determined to be reasonable. Since the specified times are likely to contribute the most erosion, they were used to determine a simulated annual rate of ~635 kg/ha. Published rates for smaller basins (McCree Creek, Burns Creek and Fox Creek) in north central Washington indicated a natural surface erosion rates of 8 – 100 kg/ha/year (Helvey, 1980). These rates were determined from weir ponds and therefore are not directly comparable to the simulated results for total surface erosion which include sediment that is not deposited in the channel network. Therefore, it is expected that the simulated result should be greater than the published rate. In addition, Rainy Creek receives more precipitation than the reference basins (58 cm at elevation 920 m) which supports the larger simulated rate.

The road erosion component was run for the entire simulation period. It was run with the minimum and maximum erodibility coefficients for raindrop detachment and overland flow (CH in equation 15), described in Smith et al. (1999). Initial runs with Ω_c set at the same value as in the hillslope erosion algorithm resulted in rates an order of magnitude lower than reported rates summarized in Table 7. Modifying Ω_c, as asserted in Section 3.2.2, increased the annual erosion rates to 17 kg/ha (minimum CH) to 41 kg/ha (maximum CH) (163-394 kg/km of road) which are more comparable to reported values. Studies performed by Cederholm et al. (1980) and Reid and Dunne (1984) in the Clearwater Basin on the Olympic Peninsula in Washington for gravel roads with various levels of use, resulted in annual road erosion rates of 3,800 to 500,000 kg/km of road (or 8, 400 to 1.11×10^{6} kg/ha of road, using the mean road width of 4.5 m). This basin receives significantly more precipitation (350 cm/year) which could explain the difference. A study by Ketcheson et al. (1999) in the Silver Creek Study Area in central Idaho, showed rates of 12,000 to

55,000 kg/ha of road, 2 to 4 years after construction. In this case the difference can not be explained by difference in precipitation since the basin receives less precipitation (90 cm/year). The difference could be that our model does not account for erosion of the total road prism area including road cut and fill. In addition, materials used to construct forest roads in Idaho break down much easier than those used in the Pacific Northwest.

5.3. Channel Routing

The simulated sediment concentration in Rainy Creek outflow ranged from 11-174 parts per million (ppm) with a mean value of 61 ppm (Figure 9). This range is reasonable when compared to observed concentrations in other Washington rivers (Table 7). The calculated sediment yield for the modeled time period is 1,000-1,020 kg/ha/year, which again is reasonable when compared to reported values (Table 8). The algorithm initializes the sediment bed depth in each channel segment. In the beginning of the model run, much of this sediment is transported out of the network. The sediment yield during this spinup period is not included in the results reported above.

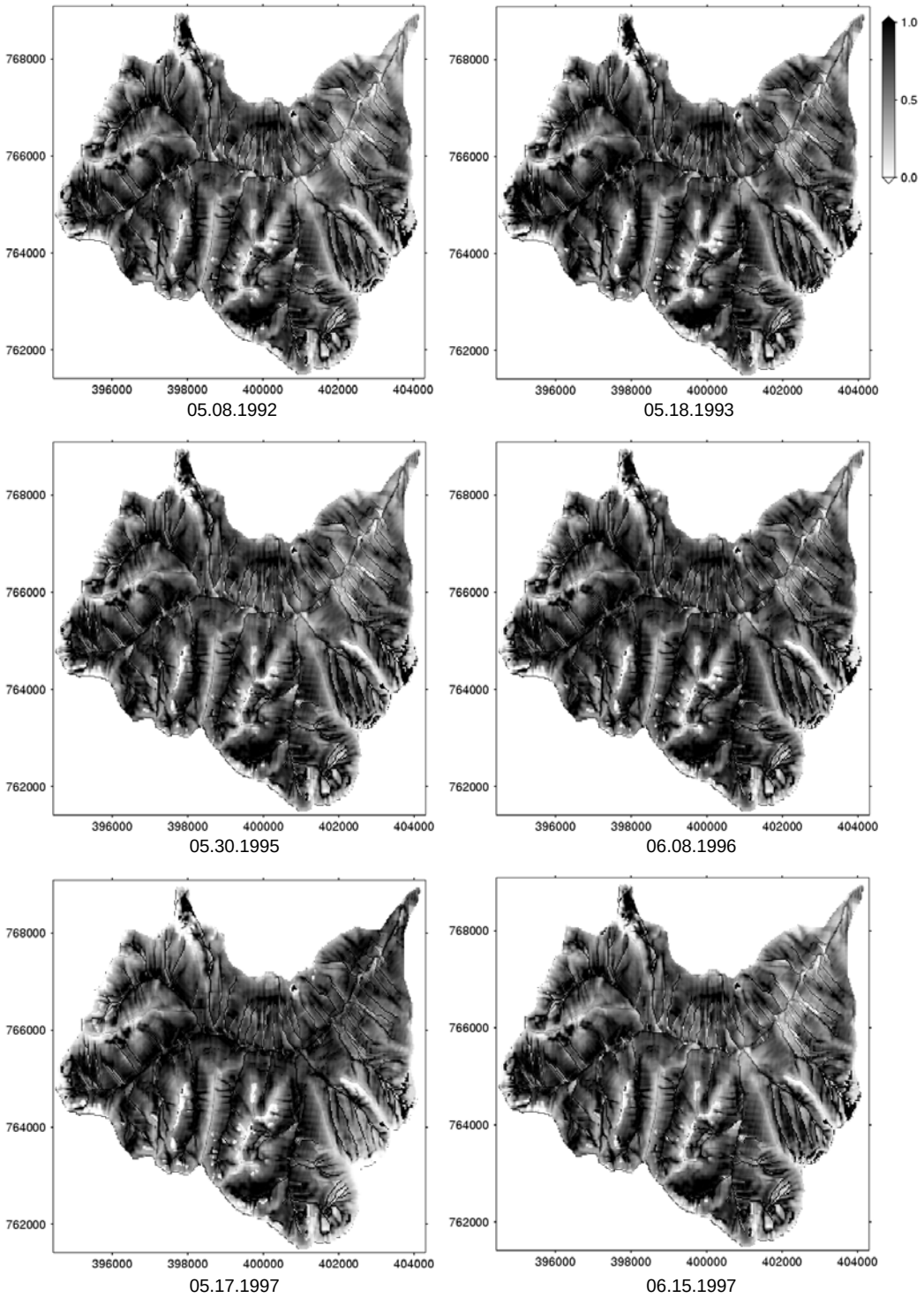

Figure 6. Modeled saturated fraction (saturated depth/soil depth) for storm events

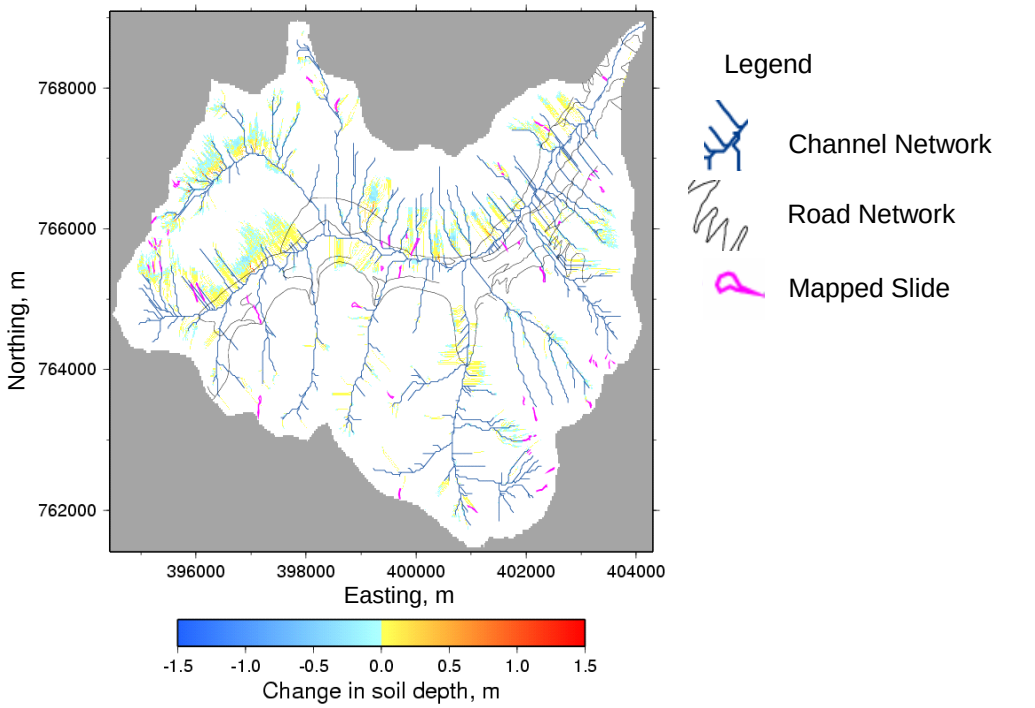

(a)

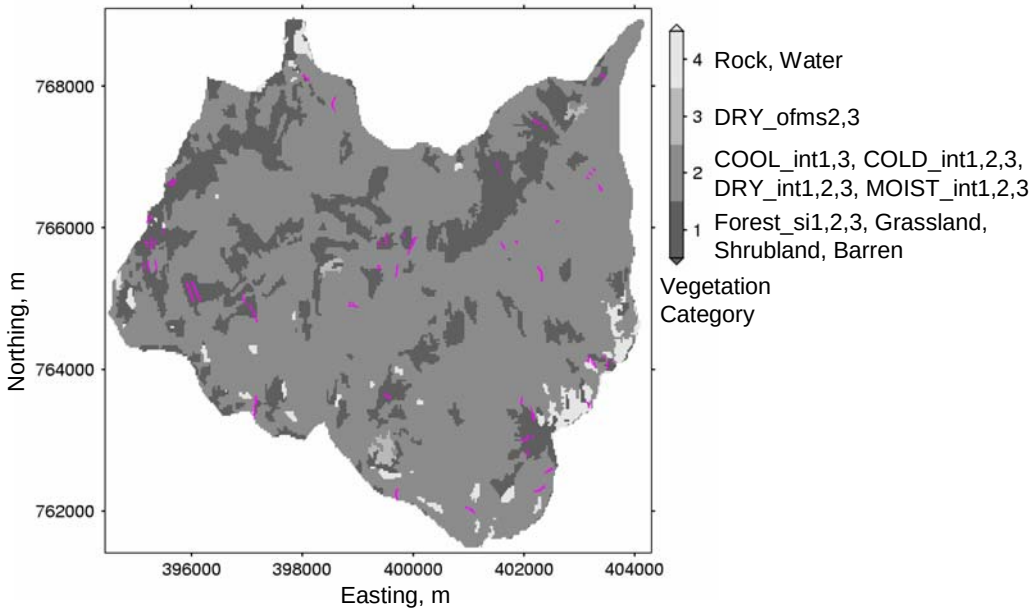

(b)

Figure 7. (a) Change in soil depth overlain with aerial photograph mapped landslides. Blue areas represent failures, while yellow/orange areas represent deposition. White area indicates no change in soil depth. (b) Year 2000 vegetation categories overlain with aerial photograph mapped landslides.

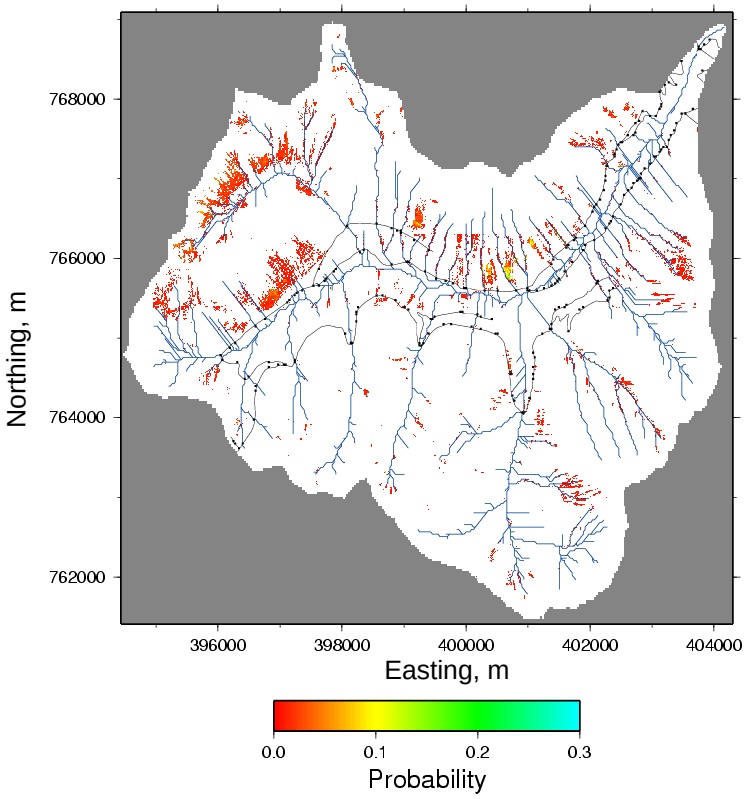

Figure 8. Maximum failure probability map. Maximum failure probability from six simulated mass wasting events. White area indicates failure probability of zero.

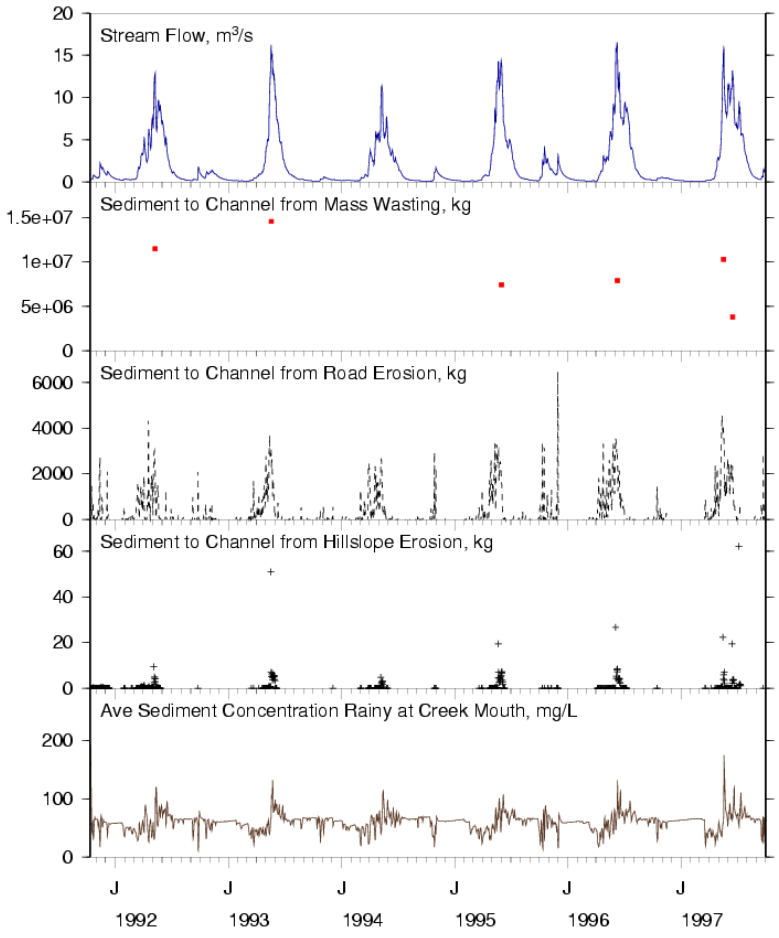

Figure 9. Modeled streamflow, sediment inputs to the channel network, and sediment concentration at Rainy Creek outflow. The mass wasting algorithm was run on 05/08/1992, 05/18/1993, 05/30/1995, 06/08/1996, 05/17/1997, and 06/15/1997. The hillslope erosion algorithm was run during periods for high modeled runoff: 05/05 - 5/12/1992; 05/18 - 05/31/1993; 05/08 - 05/15/1994; 05/21 - 06/06/1995; 06/04 - 06/18/1996; 05/16 - 05/21/1997; 06/14 - 06/20/1997; 07/06 - 07/12/1997. Peaks in sediment concentration occur with peaks in stream flow and sediment inputs from mass wasting.

Table 6. New slides determined from aerial photograph survey

Confidence Level	1970-1975	1975-1979	1979-1986	1986-1992	Area, m^2/year	Volume, m^3/year	Rate, kg/ha/year
High	1	2	0	2	579	817	296
Medium	0	3	2	5	3017	4242	1535
Low	2	6	1	6	2629	3328	1204
Total	3	11	3	13	6225	8386	3035

NOTE: See Appendix E for aerial photograph survey methodology

Table 7. Reported suspended sediment concentrations

Station Name/ID	Latitude/ Longitude	Basin Area, km^2	Days of Record	Days Missing	Max, ppm	Mean, ppm
North River Above Joe Cr, Nr Raymond, WA 12016600	46º51'40" 123º44'00"	490	365 (10/1/1964–9/30/1965)	0	210	17
Skookumchuck River Near Bucoda, WA 12026400	46º46'20" 122º55'23"	290	1,095 (10/1/1968–9/30/1971)	16	376	13
Wynoochee River Nr Grisdale, WA 12035400	47º22'50" 123º36'31"	107	485 (2/1/66–5/31/67)	21	1500	25
Clearwater Creek Near Mouth Near Cougar, WA 14216300	46º12'07" 122º00'54"	85	2,358 (1/1/82–9/30/88)	107	14,200	-
Muddy River Ab Clear Cr Nr Cougar, WA 14216350	46º07'03" 122º00'24"	218	7,30 (10/1/81–9/30/83)	120	52,600	-

Table 8. Reported sediment yield

Basin	Location	Basin Area, km^2	Mean Annual Precipitation, cm	Elevation Range, m	Mean Annual Suspended Sediment Yield, Mg/ha	Water Years
Deschutes River	Western Washington	410	100-380	0-910	0.409	1971-73
Eel River	Northern California Coast Range	750	120	560-2,130	3.42	1920-59
Flynn Creek	Oregon Coast Range	2	250	N/A	0.984	1959-73
N. Fork Cache Creek	Northern California Coast Range	510	80-130	400-1,480	2.11	1960-63
Nisqually River	Western Washington	1,120	100-510	0-4,390	0.813	1971-73
Skykomish River[2]	Western Washington	2,160	130-260	180-2,440	13.5	1967-69
Snoqualmie River[2]	Western Washington	1,561	130-260	180-2,440	3.35	1967-69

NOTES:
1. All from Larson and Sidle (1980), except where noted.
2. From Nelson (1971)

6. IMPLEMENTATION OF LAND MANAGEMENT CHANGES

For all scenarios, the mass wasting algorithm was run for the six events specified in Section 5.1. The surface erosion algorithm was run for time periods specified in Section 5.2 and the road erosion algorithm was run for the entire simulation period.

6.1. Road Scenarios

The model was run for two road scenarios to evaluate the differences in 1) simulated failure probability (location and magnitude) resulting from road location on the hillslope, and 2) road surface erosion for varying road density. The scenarios were a partially decommissioned network and no road network, and they were compared to the initial run with the existing road network. The partially decommissioned network was created in ArcInfo by using the existing network and culvert locations, and then removing segments prescribed by the USDA Forest Service. The summary statistics of the initial run and these scenarios are provided in Table 9. Relative to past assessments of the effects of forest roads on basin hydrology using DHSVM, the road density of 1.05 km/km^2 in Rainy Creek is small. In particular, LaMarche and Lettenmaier (1998) and Bowling and Lettenmaier (2001) used DHSVM to model the Deschutes River subbasins, which had road densities that varied from 3.2 to 5.0 km/km^2. Their simulations showed an increase in peak flows and an average change in peaks over threshold from 1.8 to 9.0 percent. While the effect of roads on basin hydrology is the result of a number of road characteristics, the larger the road network the greater the potential for observable changes in hydrology. The relatively small change in the road network for the road scenarios in Rainy Creek showed less than a one percent change in annual peak flows. There were minor changes (average from 0.02 to 0.03) in simulated saturated fraction (saturated depth/soil depth) for the mass wasting events. The areas these differences in saturated fraction were simulated are shown on Figure 10.

In order to isolate the effects of forest roads on simulated basin hydrology and thus probability of failure, the scenarios were run so that, for each iteration, all grid cells with the same vegetation class or soil classes were assigned the same parameters from the input distributions. This differs from the initial run, where every time the FS was calculated random values were used, resulting in spatially and temporally varying parameters for the same vegetation and soil classes. The results of scenarios are summarized in Table 10. Simulated basin average road

erosion decreased with decreasing road area as expected. Road erosion rates per unit road area increased with road area, because not all road segments have enough surface runoff to cause erosion and partial decommissioning was intended to remove segments with high erosion rates. Hillslope erosion increased with decreasing road area, due to longer flow paths. Since the differences in road erosion rate are greater than the differences in hillslope erosion, however, sediment yield increases with increasing road area.

Figures 11 and 12 show the difference (existing – scenario) in the change in sediment depth and maximum failure probability, respectively, for each scenario. While the computed failure rates are similar, the spatial distribution of change in soil depth and failure probability differs, due to the effects of the road network on basin hydrology. Prior empirical studies typically report an increase in mass wasting with increasing road density, but the model does not represent some aspects of road/hydrology interaction, such as culvert blockage, and/or overtopping that can lead to the failure of roads themselves, including cut and fill slopes, and these mechanisms may dominate the observed changes. The modest changes simulated could also be attributed to small road density: the changes in soil moisture are not great enough to result in a difference in annual landsliding rate, either observed or simulated. As previously mentioned, the magnitude of the effect of roads on basin hydrology is a function of a number of characteristics, i.e. location in the hillslope and upslope contributing area, depth of road-side ditches, culvert spacing and road drainage connectivity to the stream network. These effects on basin hydrology, in turn, affect the probability of failure by causing changes in soil moisture. The density of culverts, either due to increased road density or road construction methods, and the culvert discharge location will determine the magnitude and location of these effects (it should be noted that the culvert locations were specified based on the assumptions stated in Section 4.1; culvert locations were not field verified). Roads concentrate flow prior to discharging it to the hillslope or the stream network. Therefore, if the discharge location is more stable and the intercepted water is from an unstable area, the simulated result will be a decrease in failure probability.

6.2. Fire Scenario

The model was run (with the existing road network) for a fire scenario to evaluate changes in erosion rates due to the effects of 1) changes in soil moisture, surface runoff and streamflow due to reduced leaf area index (LAI) and loss of understory, and 2) reduction in root cohesion. The

fire was simulated by removing the understory from all pixels with an overstory, setting the LAI of pixels with an overstory to1.0, and reducing the root cohesion distributions of the pixels with an overstory was reduced by 2 kPa, simulating the loss of the understory. Woody shrubs and groundcover typically have root cohesion < 3 kPa (Montgomery et al., 1998). These modifications were held constant throughout the six-year simulation. Hydrology model initial conditions for soil, snow, precipitation intercepted by the vegetation, and channel flow were the same for both runs. They were taken as the final model conditions from a two-year run of the model (10/01/1989 – 9/30/1991) with current vegetation and roads. Also, for both runs overland flow road erodibility coefficient CH for road erosion was set at 0.02.

Figure 13 shows the modeled streamflow, sediment inputs to the channel network, and sediment concentration of Rainy Creek for this scenario. Figures 14 and 15 show the difference (existing – fire) in changes in sediment depth and maximum failure probability, respectively. The results are summarized in Table 11. The fire scenario results in decreased evapotranspiration due to reduced LAI. Total simulated streamflow increased by nine percent, surface runoff increased by thirteen percent, but the average saturated area in the basin increased by only 0.08 percent. The mass wasting rate increased by 56 % due to the decreased root cohesion. Most (65%) of the additional failed material was deposited on the hillslope while 35% was delivered to the channel network. The hillslope erosion rate increased due to more particle detachment from additional raindrop and leaf drip energy due to the removal of the understory, and increased runoff and thus transport capacity. Due to decreased LAI of the overstory and loss of the understory, less precipitation was intercepted by the overstory resulting in more precipitation reaching the road surface. This results in higher road runoff, because there is no infiltration on the road surface. The road erosion rate increased due to the additional runoff and transport capacity. Peak concentrations, following each of the mass wasting events, increased by 11.5 to 51.9 percent for four out of the six events. The remaining two events showed a decrease of less than five percent.

Sediment yield, however, did not increase in proportion to the additional inputs to the channel network. For the existing conditions simulation, 86% of the sediment inputs to the channel network remained in channel storage. For the fire scenario this increased to 95% and includes most of the additional failed material. Colluvium may accumulate in low order channel segments between episodes of debris flow scour (e.g. Benda, 1990). Sediments may also accumulate due to temporary storage in tributary junctions, fans and terraces. However, in my simulations, debris

flows do not remove all sediment in the channel segments they flow through, which is somewhat unrealistic. If they did, the sediment yield would increase. Moreover, the channel routing module does not account for changes in channel slope or morphology resulting from large sediment inputs. Accounting for such effects would tend to reduce channel storage over the simulation period.

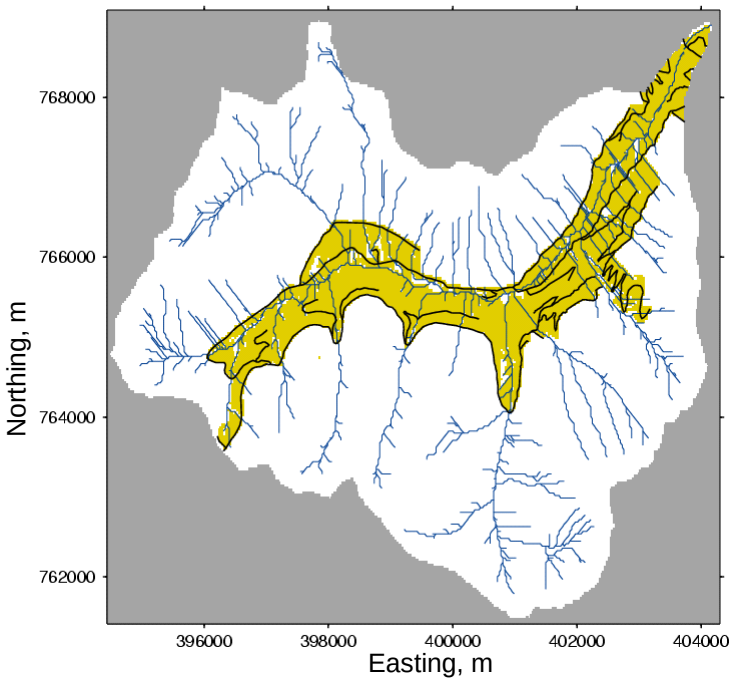

Figure 10. Basin area with change in saturated fraction (saturated depth/soil depth) for road scenarios

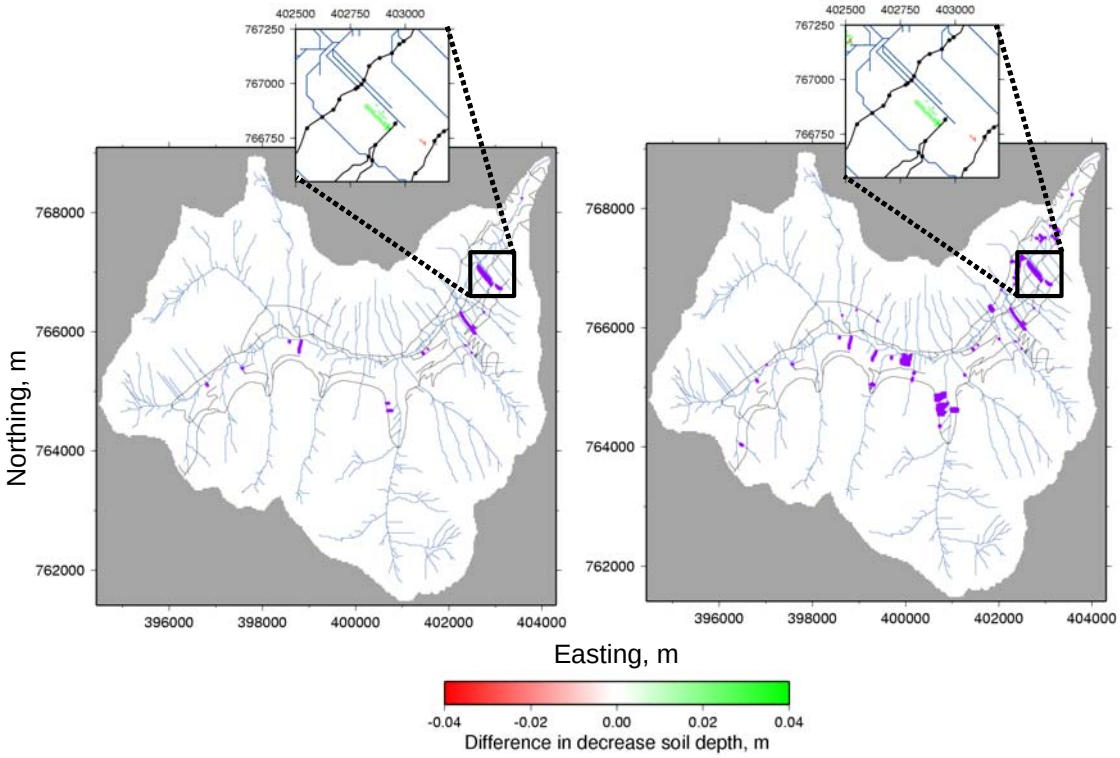

Figure 11. Difference in decrease in soil depth (a) existing - partially decommissioned road network (b) existing - no roads. Purple areas mark all areas with differences in changes in soil depth. A modified range is shown for clarity. The full range of differences is -0.098 to 0.04 m for existing - partially decommissioned road network and -0.132 to 0.01 m for existing - no roads.

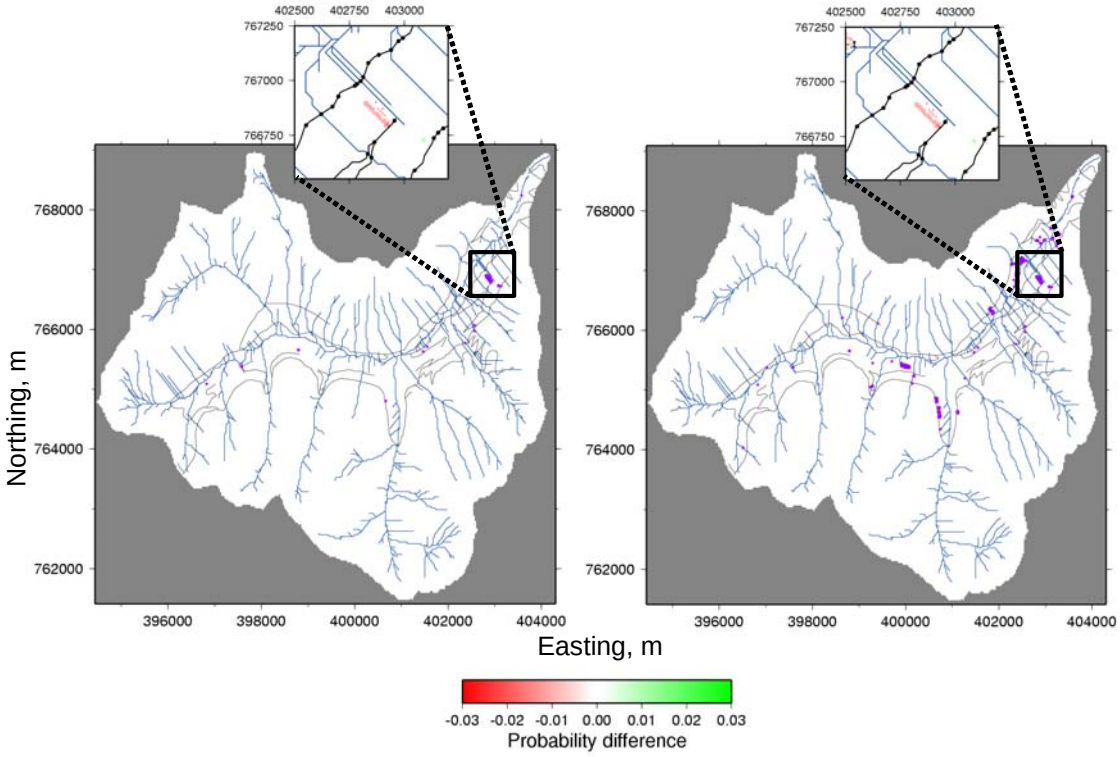

Figure 12. Difference in maximum event probability of failure (a) existing - partially decommissioned road network (b) existing - no roads. Purple areas mark all areas with changes. Green indicates a larger probability of failure for the existing conditions.

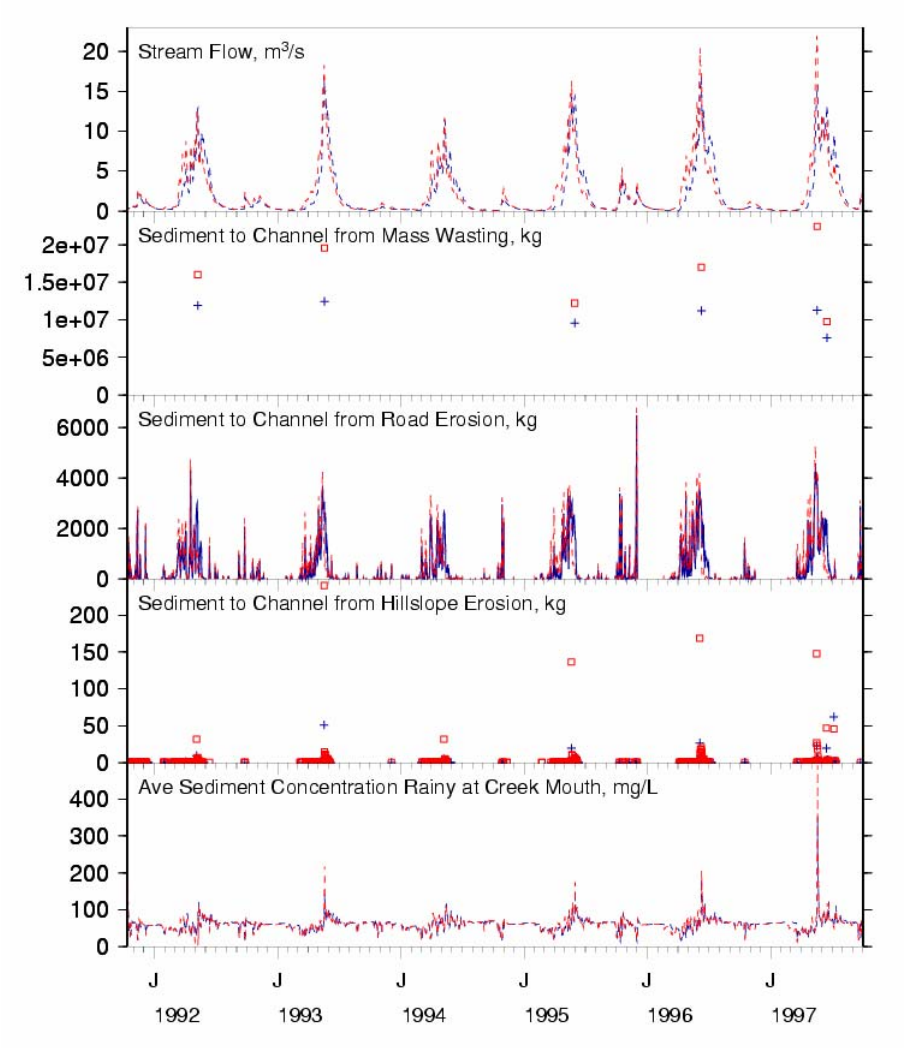

Figure 13. Fire scenario modeled streamflow, sediment inputs to the channel network and sediment concentration at Rainy Creek outflow. The existing run is in blue and the fire scenario is in red. The fire scenario resulted in higher streamflows, greater sediment inputs into the channel network, and larger peak sediment concentration for four of the six peaks following mass wasting events.

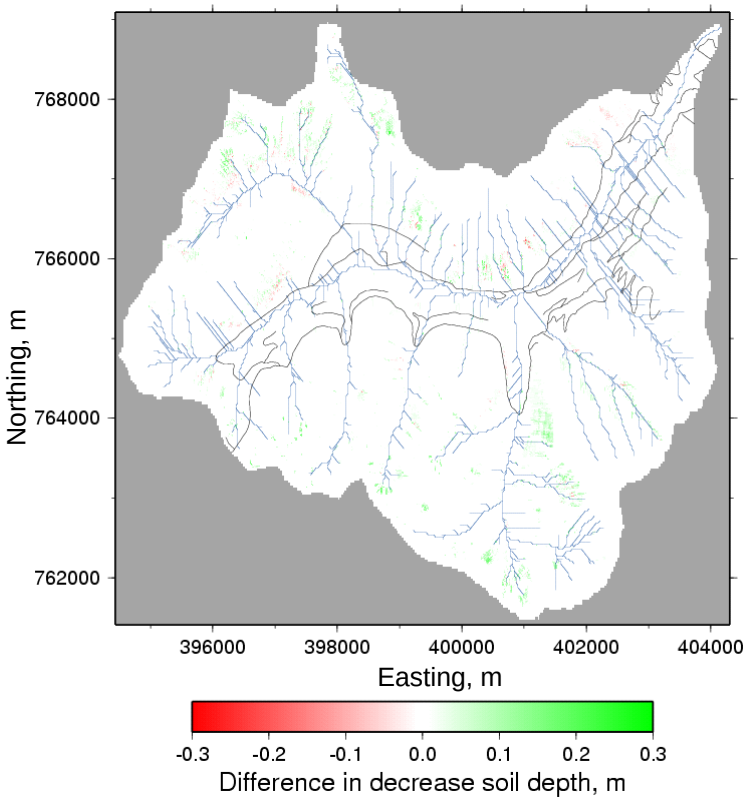

Figure 14. Difference (existing – fire) in decrease (mass wasting) in soil depth. Negative (positive) value means existing had larger (smaller) failure.

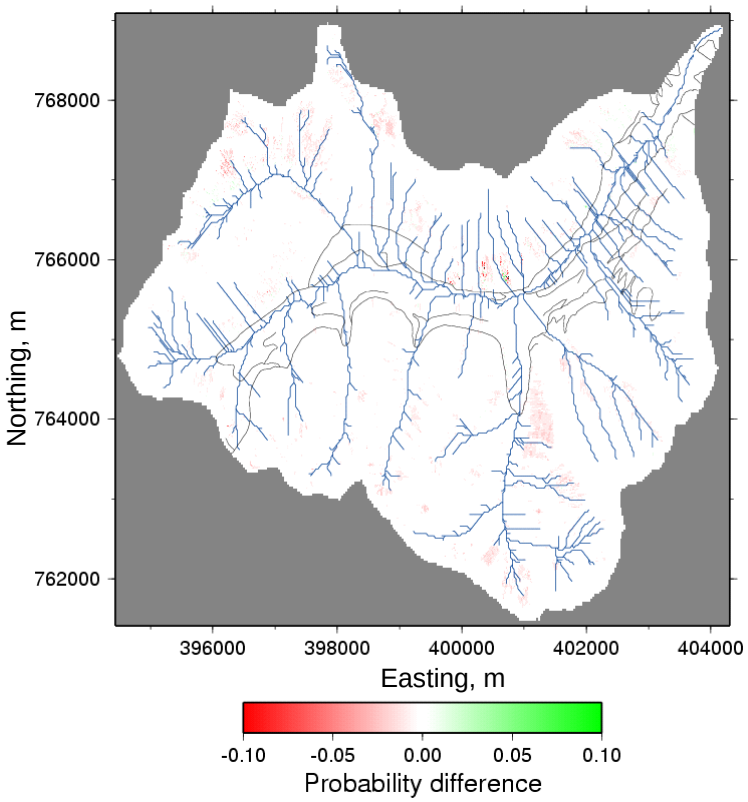

Figure 15. Difference (existing – fire) in maximum event probability of failure. The difference ranged from -0.12 to 0.26, but a modified range is shown for clarity. Red indicates a creating probability of failure for the fire scenario.

Table 9. Road scenarios

Road Network	Road Density, km/km^2	Number of Culverts	Total Road Surface Area, km^2	% Area by Class 106	515	518
Existing	1.05	284	0.23	10.36	40.00	49.64
Partially Decommissioned	0.75	202	0.17	< 1	30.53	69.45
None	0	0	0	0	0	0

Table 10. Road scenario results – basin average annual rates

Road Network	Sediment Yield Mg/ha	Landslide Rate, kg/ha[1]	Hillslope Erosion Rate, kg/ha[2]	Road Erosion Rate kg/ha	kg/km of road
Existing	1.00-1.02	6,745	635	17-41 (3,247–7,842)[3]	163-394
Partially Decommissioned	0.99	6,750	636	2-6 (556-1,537)[3]	20-57
None	0.97	6,765	643	0	0

NOTES:
1) The mass wasting algorithm was run on 05/08/1992, 05/18/1993, 05/30/1995, 06/08/1996, 05/17/1997, and 06/15/1997.
2) The hillslope erosion algorithm was run during periods for high modeled runoff: 05/05 - 5/12/1992; 05/18 - 05/31/1993; 05/08 - 05/15/1994; 05/21 - 06/06/1995; 06/04 - 06/18/1996; 05/16 - 05/21/1997; 06/14 - 06/20/1997; 07/06 - 07/12/1997. Since these times are likely to contribute the most erosion, they were used to determine the annual rate.
3) Value in parenthesis is road erosion rate per hectare of road area.

Table 11. Fire scenario results – basin average annual rates

Scenario	Sediment Yield Mg/ha	Landslide Rate, kg/ha[1]	Hillslope Erosion Rate, kg/ha[2]	Road Erosion Rate kg/ha	kg/km of road
Existing	1.01	6,745	635	34 (6,377)[3]	320
Fire	1.09	10,530	1,416	37 (7,093)[3]	356

NOTES:
1) The mass wasting algorithm was run on 05/08/1992, 05/18/1993, 05/30/1995, 06/08/1996, 05/17/1997, and 06/15/1997.
2) The hillslope erosion algorithm was run during periods for high modeled runoff: 05/05 - 5/12/1992; 05/18 - 05/31/1993; 05/08 - 05/15/1994; 05/21 - 06/06/1995; 06/04 - 06/18/1996; 05/16 - 05/21/1997; 06/14 - 06/20/1997; 07/06 - 07/12/1997. Since these times are likely to contribute the most erosion, they were used to determine the annual rate.
3) Value in parenthesis is road erosion rate per hectare of road area.

7. CONCLUSIONS

We have presented an approach to predicting erosion and sediment transport using DHSVM. My approach includes the main sources of sediment supply: mass wasting, hillslope erosion, and forest road erosion in forested mountainous watersheds. It includes sediment routing from these sources to the stream channel network as well as routing through the network so that basin sediment yield can be determined. It can be used to model the relative effects of forest road construction and decommissioning as well as vegetation changes, such as harvesting and forest fires. We have shown through a test application to the Rainy Creek catchment that the model produces plausible sediment yields in comparison with literature values for similar catchments, and ratios of landsliding and surface erosion rates that are plausible when compared to published rates for various watersheds in the Pacific Northwest.

The model was applied to compare the effects of reducing road densities on erosion and sediment transport in the Rainy Creek drainage. This scenario showed only small changes in mass wasting rates and sediment yield, and some spatial changes in mass wasting locations. Also, as road density decreased the road erosion rate/road area decreased. Larger changes were not realized, either due to the limited hydrologic changes caused by the roads, the construction of roads at low elevation along the main channel, or because road characteristics that contribute to road-related mass wasting (i.e. blocked culverts) are not represented in the model. A second scenario, representing a forest fire, showed an increase in all erosion components due to decreases in root cohesion and increases in surface runoff and thus transport capacity. The increase in sediment yield was not proportional to the increase in sediment inputs, however, because the channel routing module retained the majority of the additional sediment in the channel network for the six year duration of the simulation.

The DHSVM sediment module requires inputs in addition to those required for the hydrologic model. Some of these data were provided by the USDA Forest Service and the remainder were obtained from published sources. Rather than using published values, site-specific data would have helped modeling efforts. These data would aid in selecting values for parameters to which the model is sensitive, as well as determining erosion rates for simulation evaluation. In addition to input requirements, site-specific data would help with the development of the sediment algorithms. For example, results of field mapping of slides could be used to

modify the rule-based redistribution of failed material, that determines sediment delivery to the channel network.

REFERENCES

Amaranthus, M.P., R.M. Rice, N.R. Barr, and R.R. Ziemer, 1985: Logging and Forest Roads Related to Increased Debris Slides in Southwestern Oregon, *Journal of Forestry*, 83, 229-233.

Ascough II, J.C., C. Baffaut, M.A. Nearing, and B.Y. Liu, 1997: The WEPP watershed model: I. Hydrology and erosion: *Transactions ASAE*, 40, 921-933.

Bagnold, R.A., 1966: An approach of sediment transport model from general physics, US Geological Survey Prof. Paper 422-J.

Benda, L., 1990, The influence of debris flows on channels and valley floors of the Oregon Coast Range, U.S.A., *Earth Surf. Process. Landforms*, 15, 457-466.

Benda, L., and T. Dunne, 1997: Stochastic forcing of sediment supply to channel networks from landsliding and debris flow, *Water Resour. Res.*, 33, 2849-2863.

Bergen, K.J., C.O. Doten, and D.P. Lettenmaier, 2003. Landslide rates in the Eastern Cascade Mountain Range, poster presented at the American Geophysical Union Fall Meeting, San Francisco.

Beven, K.J. and M.J. Kirkby, 1979: A physically based, variable contributing area model of basin hydrology, *Hydrological Sciences Bulletin*, 24, 43-69.

Borga, M., G. Dalla Fontana, C. Gregoretti, and L. Marchi, 2002: Assessment of shallow landsliding by using physically based model of hillslope stability, *Hydrol. Process.*, 16, 2833-2851.

Bowling, L.C., and D.P. Lettenmaier, 1997: Evaluation of the effects of forest roads on streamflow in Hard and Ware Creeks, Washington, Water Resources Series Technical Report No. 155, Department of Civil and Environmental Engineering, University of Washington.

Bowling, L.C. and D.P. Lettenmaier, 2001: The effects of forest roads and harvest on catchment hydrology in a mountainous maritime environment, In: Wigmosta, M.S. and S.J. Burges, (eds), Land Use and Watersheds: Human Influence on Hydrology and Geomorphology in Urban and Forest Areas, AGU Water Science and Application Volume 2, p. 145-164.

Burroughs, E.R., Jr. and B.R. Thomas, 1977: Declining root strength in Douglas-Fir after felling as a factor in slope stability. Res. Pap. INT-190, Ogden, UT. US Depart. of Agriculture, Forest Service, Intermountain Forest and Range Experiment Station, 27 p.

Burton, A. and J.C. Bathurst, 1998: Physically based modeling of shallow landslide sediment yield at a catchment scale, *Environmental Geology*, 35, 89-99.

Burton, A., T.J. Arkell, and J.C. Bathurst, 1998: Field variability of landslide model parameters, *Environmental Geology*, 35, 110-115.

Chow, V.T., D.R. Maidment, and L.W. Mays, 1988: *Applied Hydrology*, McGraw Hill, New York, 572 pp.

Daly, C., R.P. Neilson, and D.L. Phillips, 1994: A statistical-topographic model for mapping climatological precipitation over mountainous terrain, *Journal of Applied Meteorology*, 33, 140-158.

Daly, C., G.H. Taylor, and W.P. Gibson, 1997: The PRISM approach to mapping precipitation and temperature, In reprints: 10th Conf. on Applied Climatology, Reno, NV, American Meteorological Society, 10-12.

Dhakal, A.S. and R.C. Sidle, 2003: Long-term modelling of landslides for difference forest management practices, *Earth Surf. Process. Landforms*, 28, 853-868.

Dietrich, R.V., J.J.T. Dutro, and R.M. Foose, 1982: *AGI Data Sheets for geology in the field, laboratory, and office*, 2nd ed., American Geological Institute, Falls Church, VA.

Dietrich, W.E. and T. Dunne, 1978: Sediment budget for a small catchment in mountainous terrain: *Z. Geomorph.,* Suppl. Bd. 29, 191-206.

Dietrich, W.E., R. Reiss, M. Hsu, and D.R. Montgomery, 1995: A process-based model for colluvial soil depth and shallow landsliding using Digital Elevation Data, *Hydrol. Process.*, 9, 383-400.

Duncan, S.H., R.F. Bilby, J.W. Ward and J.T. Heffner, 1987: Transport of Road-Surface Sediment Through Ephemeral Stream Channels, *Wat. Resour. Bull.*, 23, 113-119.

Engman, E.T., 1986: Roughness coefficients for routing surface runoff, *Journal of Irrigation and Drainage Engineering*, ASCE,112, 39-53.

Exner, F.M., 1925: Ber die wechselwirkung zwischen wasser und geschiebe inflssen, *Sitzungber. Acad. Wissenscaften Wien Math. Naturwiss* Abt. 2a,134, 165-180.

Graf, W., 1971: *Hydraulics of Sediment Transport*, McGraw-Hill, New York, pp. 208-211.

Gray, W.H. and W.F. Megahan, 1981, Forest vegetation removal and slope stability in the Idaho batholith, *Res. Pap. INT-271*, USDA For. Serv., Ogden, Utah.

Gonzalez-Bonorino, G., and W.R. Osterkamp, 2004: Applying RUSLE 2.0 on burned-forest lands: An appraisal, *Journal of Soil and Water Conservation*, 59, 36-42.

Govers, G., 1992: Evaluation of transporting capacity formulae for overland flow, In: Overland Flow: Hydraulics and Erosion Mechanics, Parsons J.A. and Abrahams A.D. Eds. UCL Press Limited, London.

Hammond, C., D. Hall, S. Miller and P. Swetik, 1992: Level I Stability Analysis (LISA) Documentation for version 2.0, USDA Intermountain Research Station, General Technical Report INT-285.

Kalnay, E. and Coauthors, 1996: The NCEP/NCAR 40-Year Reanalysis Project. *Bull. Amer. Meteor. Soc*., 77, 437-471.

Helvey, J.P., 1980, Effects of a North Central Washington Wildfire on Runoff and Sediment Production, *Water Resources Bulletin*, l6, 627-634.

Ketcheson, G.L., W.F. Megahan, and J.G. King, 1999: "R1-R4" and "BOISED" Sediment Production Model Tests using Forest Roads in Granitics, *J. Amer. Water Resour. Assoc.,* 35, 83-98.

KINEROS2 model documentation (http://www.tucson.ars.ag.gov/kineros/Docs/DocNav.html#)

Koler, T.E., 1998: Evaluating slope stability in forest uplands with deterministic and probabilistic models, *Environmental and Engineering GeoScience*, 4, 185-194.

Komura, W., 1961: Bulk properties of river sediments and their application to sediment hydraulics, *Proc. Jap. Nat. Cong. For Appl. Mech*.

LaMarche, J., and D.P. Lettenmaier, 1998: Forest Road Effects on Flood Flows in the Deschutes River Basin, Washington, Water Resources Series, Technical Report 158, University of Washington, Seattle.

LaMarche, J., and D.P. Lettenmaier, 2001: Effects of Forest Roads on Flood Flows in the Deschutes Basin, Washington, *Earth Surf. Process. Landforms*, 26, 115-134..

Larson, K. R., and R.C. Sidle, 1980: Erosion and sedimentation data catalog of the Pacific Northwest. U.S. Department of Agriculture Forest Service, Pacific Northwest Region, R6-WM-050-1981, Portland, Oregon.

Leung, L.R., and M.S. Wigmosta, 1999: Potential climate change impacts on mountain watersheds in the Pacific Northwest, *J. Amer. Water Resour. Assoc.*, 35, 1463-1471.

Maurer, E.P., A.W. Wood, J.C. Adam, D.P. Lettenmaier, and B. Nijssen, 2002: A long-term hydrologically-based data set of land surface fluxes and states for the conterminous United States, *Journal of Climate,* 15, 3237-3251.

Montgomery, D.R. and W.E. Dietrich, 1994: A physically based model for topographic control on shallow landsliding, *Water Resour. Res.*, 30, 1153-1171.

Montgomery, D.R., K. Sullivan, and H.M. Greenberg, 1998: Regional test of a model for shallow landsliding, *Hydrol. Process.*, 12, 943-955.

Morgan, R.P.C., J.N. Qinton, R.E. Smith, G. Govers, J.W.A. Poesen, K. Auerswald, G. Chisci, D. Torri and M.E. Styczen, 1998: The European soil erosion model (EUROSEM): a dynamic approach for predicting sediment transport from fields and small catchments, *Earth Surf. Process. Landforms*, 23, 527-544.

Nelson, L.M., 1971, Sediment Transport by Stream in the Snohomish River Basin, Washington October 1967 – June 1969, United States Department of the Interior Geological Survey Open File Report .

Nijssen, B., I. Haddeland, and D.P. Lettenmaier, 1997: Point evaluation of a surface hydrology model for BOREAS, *J. Geophys. Res.,* 102, 29,367-29,378.

Reid, L.M., and T. Dunne, 1984: Sediment production from forest road surfaces, *Water Resour. Res.*, 29, 1753-1761.

Reiners, P.W., T.A. Ehlers, S.G. Mitchell, and D.R. Montgomery, 2003, Coupled spatial variation in precipitation and long-term erosion rates across the Washington Cascades, *Nature*, 426, 645-647.

Reneau, S.L. and W.E. Dietrich, 1987: Size and location of colluvial landslides in a steep forested landscape, In: Beschta R.L., T. Blinn, G.E. Grant, G.G. Ice, and F.J. Swanson (eds), Erosion and sedimentation in the Pacific Rim, IAHS Publ. No. 165, Institute of Hydrology, Wallingford, Oxfordshire, UK.

Rubey, W.W., 1933: Settling velocities of gravels, sands, and silt particles, *Am. Journal of Science, 5th Series*, 25, 325-338.

Schmidt, K.M., J.J. Roering, J.J. Stock, W.E. Dietrich, D.R. Montgomery, and T. Schaub, 2001: Root cohesion variability and shallow landslide susceptibility in the Oregon Coast Range, *Can. Geotech, J.*, 38, 995-1024.

Selby, M.J., 1982, Hillslope materials and processes, Oxford [Oxfordshire]; New York: Oxford University Press.

Sidle, R.C., A.J. Pearce, and C.L. O'Loughlin, 1985, Hillslope stability and land use. Water Resources Monograph Series 11, American Geophysical Union, Washington D.C.

Smith, R.E. and J.Y. Parlange, 1978: A parameter-efficient hydrologic infiltration model, *Water Resour. Res.*, 14, 533-538.

Smith, R.E., D.C. Goodrich, D.A. Woolhiser, and C.L. Unkrich, 1995: KINEROS – a kinematic runoff and erosion model, In: Singh, V.P. (ed), Computer Models of Watershed Hydrology, Water Resources Publication, Highland Ranch, Colorado, pp. 697-732.

Smith, R.E., D.C. Goodrich and C.L. Unkrich, 1999: Simulation of selected events on the Catsop catchment by KINEROS2, A report for the GCTE conference on catchment scale erosion models, *Catena,* 37, 457-475.

Storck, P., D.P. Lettenmaier, B.A. Connelly, and T.W. Cundy, 1995: Implications of forest practices on downstream flooding, phase II final report, University of Washington, Seattle.

Storck, P., L. Bowling, P. Wetherbee and D. Lettenmaier, 1998: Application of a GIS-based distributed hydrology model for prediction of forest harvest effects on peak stream flow in the Pacific Northwest, *Hydro. Process.,* 12, 889-904.

Storck P., and D.P. Lettenmaier, 2000: Trees, snow and flooding: An investigation of forest canopy effects on snow accumulation and melt at the plot and watershed scales in the Pacific Northwest, Water Resources Series Technical Report No. 161, Department of Civil and Environmental Engineering, University of Washington.

Sturm, T., 2001: *Open Channel Hydraulics*, McGraw-Hill, New York, pp. 378-380.

Tarboton D.G., R.L. Bras, and I. Rodriguez-Iturbe, 1991: On the Extraction of Channel Networks from Digital Elevation Data, *Hydrol. Process.*, 5, 81-100.

Ward, T.J., R. Li, and D.B. Simons, 1981: Use of a mathematical model for estimating potential landslide sites in steep forested drainage basins, In: Erosion and sediment transport in Pacific Rim steeplands, T.R.H. Davies ad A.J. Pearce (eds), IAHS Publ. No. 132, Institute of Hydrology, Wallingford, Oxfordshire, UK

Ward, T.J., R. Li, and D.B. Simons, 1982: Mapping landslide hazards in forest watersheds, *Journal of the Geotechnical Engineering Division*, ASCE, 108(GT2), 319-324.

Whitaker, A.Y., Y. Alila, J. Beckers, and D. Toews, 2002: Evaluating peak flow sensitivity to clear-cutting in different elevation bands of a snow-melt dominated mountainous catchement, *Water Resour. Res.*, 38, 1172.

Whitaker, A.Y., Y. Alila, J. Beckers, and D. Toews, 2003: Application of the distributed hydrology, soil vegetation model to redfish creek, British Columbia: model evaluation using internal catchment data, *Hydro. Process.*, 17, 199-224.

Wicks, J.M. and J.C. Bathurst, 1996: SHESED: a physically based, distributed erosion and sediment yield component for the SHE hydrological modeling system, *Journal of Hydrology*, 175, 213-238.

Wigmosta, M.S., L.W. Vail, and D.P. Lettenmaier, 1994: A distributed hydrology-vegetation model for complex terrain, *Water Resour. Res.,* 30, 1665-1669.

Wigmosta M.S. and D.P. Lettenmaier, 1999: A comparison of simplified methods for routing topographically-driven subsurface flow, *Water Resour. Res.*, 35, 255-264.

Wigmosta, M.S. and W.A. Perkins, 2001: Simulating the effects of forest roads on watershed hydrology, In: Land Use and Watersheds: Human Influence on Hydrology and Geomorphology in Urban and Forest Areas, M.S. Wigmosta and S.J. Burgess (eds), AGU Water Science and Application, V.2, p. 127-143.

Wolock, D.M. and G.J. McCabe Jr., 1995: Comparison of single and multiple flow direction algorithms, *Water Resour. Res.*, 31, 1315-1324.

Woolhiser, D.A., 1975: Simulation of unsteady overland flow, Mahmood, K. and V. Yevjevich (eds), Unsteady Flow in Open Channels, V.II, Water Resources Publications, Fort Collins, CO., p. 502.

Woolhiser, D.A., R.E. Smith and D.C. Goodrich, 1990: KINEROS, A kinematic runoff and erosion model: documentation and user manual, USDA-Agricultural Research Service, ARS-77, 130 pp.

Wu, T.H., 1984: Effect of vegetation on slope stability. Transportation Res. Rec. 965. Washington, DC: Transportation Research Board. 37-46.

Wu, T.H., W.P. McKinnel and D.N. Swanston, 1979: Strength of tree roots and landslides on Prince of Wales Island, Alaska, *Can. Geotech. J.*, 16, 19-33.

Wu, W., and R.C. Sidle, 1995: A distributed slope stability model for steep forested basins, *Water Resour. Res.*, 31, 1097-2110.

Ziegler, A.D., T.W. Giambelluca, and R.A. Sutherland, 2001: Erosion prediction on unpaved mountain roads in northern Thailand: validation of dynamic erodibility modeling using KINEROS2, *Hydrol. Process.*, 15, 337-358.

Ziemer, R.R., 1981: Roots and stability of forested slopes, In: Davies, T.R.H. and A.J. Pearce (eds), Erosion and Sediment Transport in Pacific Rim Steeplands, IAHS Publ. No. 132, Institute of Hydrology, Wallingford, Oxfordshire, UK.

APPENDIX A – NOTATION

ϕ effective angle of internal friction of soil on impermeable layer, degrees.
θ time weighting factor.
ω stream power per unit bed area, J/s/m^2.
β_{de} detachment efficiency.
γ_m weight density of soil at field moisture content, kg/m^3.
γ_{sat} weight density of saturated soil, kg/m^3.
γ_w weight density of water, kg/m^3.
Δt solution time step based on the Courant condition, s.
Δx grid cell dimension or stream segment length, m.
Δy grid cell dimension, m.
θ_i soil moisture content when ponding first started, fraction.
θ_s effective saturation, approximated as the porosity, fraction.
λ bed porosity.
ρ density of water, kg/m^3.
ρ_s density of particle, kg/m^3.
φ space weighting factor.
Ω stream power, m/s.
Ω_c critical stream power, m/s.
A cross-sectional area of flowing water, m^2.
c_g transfer rate coefficient, 1/T.
C current local sediment concentration, m^3/m^3.
C_d drag coefficient.
C_r root cohesion, kg/m^2.
C_s effective soil cohesion, kg/m^2.
CH road surface erodibility coefficient.
d soil depth above failure plane, m.
d_{50} median particle diameter, m.
D channel flow depth, m.
D_r soil detached by raindrop impact, kg/m^{2}s.
D_{of} soil detached by overland flow, kg/m^{2}s.
e net erosion, m^2/s.
e_b function of the mean flow velocity.
f constant that relates transmissivity to depth.
f_c infiltration rate after ponding, m/s.
FS factor of safety.
g acceleration due to gravity, m/s^2.
G mean capillary drive, m.
h surface water depth, m.
i saturation and infiltration excess, m^3/s/m.
I mean value of the topographic index.
I_i topographic index for the fine grid cell.
Inf cumulative amount of infiltrated water since ponding started, m.

K_s hydraulic conductivity, m/s.
L_{flow} road length in the direction of flow, m.
m relative saturated depth, fraction.
m_s mass of sediment stored in the bed per meter of channel length, kg/m.
n Manning's roughness coefficient.
q_0 vegetative surcharge per unit plan area, kg/m^2.
q_s local volumetric sediment inflow rate to the reach per meter of channel length, m^3/s/m.
Q inflow of water, m^3/s.
Q_i runoff from the current grid cell, m^3/s.
Q_{i-1} runoff from the grid cell upslope, m^3/s
Q^t runoff from the current time step, m^3/s.
Q^{t-1} runoff from the prior time step, m^3/s.
Q_s total sediment transport capacity, dry mass per unit width, kg/m/s.
R_n Reynold's number.
S grid cell slope, m/m.
S_c channel energy gradient, m/m.
S_{crown} road crown slope, m/m.
S_{flow} road surface slope in the direction of flow, m/m.
S_{road} road surface slope in longitudinal direction, m/m.
SG specific gravity.
$\tan\alpha$ function of the dimensionless bed shear stress.
TC transport capacity, m^3 sediment/m^3 water.
TC_c total sediment transport capacity in immersed weight per meter of channel width.
u surface water flow velocity, m/s.
v kinematic viscosity, m^2/s.
v_s particle settling velocity, m/s.
V_{ss} particle settling velocity in channel, m/s.
V average channel flow velocity, m/s.
W_c channel segment width, m.
W_r road segment width, m.
z channel bed sediment depth, m.
z' mean value of z_i', m.
z_i' potential soil moisture deficit in the fine grid cell, m.

APPENDIX B – SEDIMENT MODULE SOIL AND VEGETATION PARAMETERS

TABLE B1. Sediment Module Soil Parameters

Soil Class	Manning's Roughness coefficient, n	K_{index}, l/Joule	d50, mm	Soil Cohesion[1]		Angle of Internal Friction		
				Mean, kPa	Standard Deviation, kPa	Distribution	Min., degrees	Max., degrees
Loamy Sand	0.013	62	2.0	15	7	Uniform	31	42
Sandy Loam	0.016	32	1.5	17	5	Uniform	30	42
Fine Sandy Loam	0.02	32	0.2	18	4.5	Uniform	31	39
Loam	0.02	30	0.1	22	8	Uniform	29	38
Organic	0.02	30	0.1	22	8	Uniform	29	38
Bedrock[2]	0.01	-	2.0	2000	0	Normal	45	45
Water[2]	0.01	-	2.0	2000	0	Normal	45	45
Fragmented Rock [2]	0.013	-	2.0	2000	0	Normal	45	45

NOTES:

1. Soil cohesion distribution was normal for all soil types.
2. Soil type parameterized to prohibit mass wasting or hillslope erosion.

APPENDIX B – SEDIMENT MODULE SOIL AND VEGETATION PARAMETERS

TABLE B2. Sediment Module Vegetation Parameters

Vegetation	Root Cohesion[1]			Vegetation Surcharge[2]	
Class	Min., kPa	Mode, kPa	Max., kPa	Min., kg/m^2	Max., kg/m^2
COLD_int1	2.0	9.5	17.0	48.9	195.4
COLD_int3	2.0	9.5	17.0	48.9	195.4
COOL_int1	2.0	9.5	17.0	48.9	195.4
COOL_int2	2.0	9.5	17.0	48.9	195.4
COOL_int3	2.0	9.5	17.0	48.9	195.4
DRY_int1	12.0	17.0	23.0	48.9	195.4
DRY_int2	12.0	17.0	23.0	48.9	195.4
DRY_int3	12.0	17.0	23.0	48.9	195.4
DRY_ofms2	12.0	17.0	23.0	48.9	195.4
DRY_ofms3	12.0	17.0	23.0	48.9	195.4
Forest_si1	6.0	14.5	23.0	48.9	195.4
Forest_si2	6.0	14.5	23.0	48.9	195.4
Forest_si3	6.0	14.5	23.0	48.9	195.4
MOIST_int1	6.0	14.5	23.0	48.9	195.4
MOIST_int2	6.0	14.5	23.0	48.9	195.4
MOIST_int3	6.0	14.5	23.0	48.9	195.4
grassland	1.0	1.5	2.0	0.0	5.0
shrubland	2.0	4.0	6.0	0.0	5.0
water	Normal: Mean = 2000, Standard Dev. = 0			Normal: Mean and Standard Dev. = 0.	
rock	Normal: Mean = 2000, Standard. Dev. = 0			Normal: Mean and Standard Dev. = 0.0	
barren	Normal: Mean = 2000, Standard. Dev. = 0			Normal: Mean and Standard Dev. = 0.	

NOTES:
1. Root cohesion distribution was triangular, except where noted.
2. Vegetation Surcharge distribution was uniform, except where noted.

APPENDIX C – SOURCES FOR SOIL DEPTH MAP

The soil depth map was compiled from four sources:
1. Soil Survey Geographic (SSURGO) Database
(http://www.ncgc.nrcs.usda.gov/branch/ssb/products/ssurgo/)
2. Vegetation data developed by Roly Redmond's group at the University of Montana. This is the result of a supervised classification of Landsat imagery that was acquired on August 1, 2000.
3. Wenatchee National Forest soil depth map. This map was derived by Carl Davis (Retired.), USDA Forest Service, Okanogan-Wenatchee National Forest, by collapsing map-units from the Cashmere Mountain Soil Survey into geomorphic map units and assigning each geomorphic unit a range of soil depths.
4. Geologic data from Schuster, J.E., C.F.T. Harris, T.T. Young, and A.C. Heinitz, 1997, Digital Geologic Map Program of the Washington Division of Geology and Earth Resources, U.S. Geological Survey Open-File Report 97-269. (http://pubs.usgs.gov/of/of97-269/schuster.html)

The SSURGO data were used for soil depths less than 59 inches. The nonvegetation classes from the Landsat data set were used to fine tune these areas with shallow or no soils. For soils deeper than 59 inches, the Wenatchee National Forest soil depth map and the glacial till deposits extracted from 1:100000 digital geologic data were used to determine the soil depth.

This information was provided by Brion Salter of the USDA Forest Service Pacific Northwest Research Station.

APPENDIX D – VEGETATION DESCRIPTION

This information was provided by Kevin James of the USDA Forest Service Pacific Northwest Research Station.

Veg Description	**Forest cover types** (see table 7 for definitions and descriptions)
COLD_int	whitebark pine, western white pine or sugar pine or both, mountain hemlock, lodgepole pine, Engelmann spruce or subalpine fir or both, western hemlock or western redcedar or both
COOL_of	western larch, mountain hemlock, Engelmann spruce or subalpine fir or both
DRY_int	ponderosa pine, Douglas-fir
DRY_ofms	ponderosa pine, Douglas-fir
DRY_ofss	ponderosa pine, Douglas-fir
Forest_si	whitebark pine, mountain hemlock, western hemlock or western redcedar or both, Engelmann spruce or subalpine fir or both, Pacific silver fir, ponderosa pine, Douglas-fir, western larch, grand fir or white fir or both, western white pine or sugar pine or both
HDWD	aspen-cottonwood-willow
MOIST_int	ponderosa pine, grand fir or white fir or both, Pacific silver fir, western larch spruce or subalpine fir or both, western hemlock or western redcedar or both, Douglas-fir, western white pine or sugar pine or both
MOIST_ofms	Pacific silver fir, western hemlock or western redcedar or both, grand fir or white fir or both

Structure classes (see table 5 for definitions and descriptions)
CoverType**_int** = combination of the following structure classes: stem exclusion open canopy, stem exclusion closed canopy, understory reinitiation, and young-forest multistory

CoverType **_si** = stand initiation

CoverType **_ofms** = old-forest multistory

CoverType **_ofss** = old-forest single story

CoverType **_of** = old-forest

Historical and Current Forest and Range Landscapes in the Interior Columbia River Basin and Portions of the Klamath and Great Basins

Part 1: Linking Vegetation Patterns and Landscape Vulnerability to Potential Insect and Pathogen Disturbances

Paul F. Hessburg, Bradley G. Smith, Scott D. Kreiter, Craig A. Miller, R. Brion Salter, Cecilia H. McNicoll, and Wendel J. Hann

Interior Columbia Basin Ecosystem Management Project: Scientific Assessment

Thomas M. Quigley, Editor

U.S. Department of Agriculture
Forest Service
Pacific Northwest Research Station
Portland, Oregon
General Technical Report PNW-GTR-458
September 1999

Table 5- Descriptions of forest structural classes modeled in the midscale ecological assessment of the interior Columbia River basin

Structural class	Definition	Description
Stand initiation	Growing space is reoccupied following a stand-replacing disturbance (e.g., fire, harvest), typically by early seral species	1 canopy stratum (may be broken or continuous); 1 cohort[a] seedlings or saplings; grasses, forbs, shrubs may be present with early seral trees
Stem exclusion open canopy	Occurrence of new tree stems is moisture limited; crowns are open growing; canopy is broken; may be maintained by frequent under-burning or density management	1 broken canopy stratum; 1 cohort; trees excluding new stems through competition; poles, small, or medium trees; understory shrubs, grasses, forbs may be present
Stem exclusion closed canopy	Occurrence of new tree stems is mostly light limited; crowns abrading, canopy is closed	Continuous closed canopy; 1 or more canopy strata; 1 cohort; lower strata, if present, are same age as upper strata; poles, small, or medium trees; understory shrubs, grasses, forbs may be present
Understory reinitiation	Second cohort established under older, typically early seral overstory; mortality in the overstory creates growing space for new trees in the understory	Broken overstory canopy; ≥ 2 canopy strata; 2 cohorts; overstory is poles, small, or medium trees; understory is seedlings, saplings, or poles
Young-forest multistory	Several cohorts have established under the influence of management or fires with mixed lethal and nonlethal effects, or by insect and disease group killing; early seral overstory large trees are generally absent as a result of harvesting or other disturbance	Broken overstory canopy; > 2 canopy strata; > 2 cohorts; large trees are absent in the overstory; stands are characterized by diverse horizontal and vertical distributions of trees and tree sizes; seedlings, saplings, poles, small, and medium trees are present
Old-forest multistory	Multicohort, multistrata stands with large, old trees	Broken overstory canopy; > 2 canopy strata; > 2 cohorts; large trees dominate in the overstory; stands are characterized by diverse horizontal and vertical distributions of trees and tree sizes; all tree sizes may be present
Old-forest single story	Single-stratum stands of large, old trees. No or few young trees are present in the understory; parklike conditions resulting from nonlethal natural or prescribed underburning or other management are the dominant feature	Broken or continuous canopy of large, old trees; 1 stratum, may be single but usually multicohort; large trees dominate the overstory; understory absent or seedlings or saplings; grasses, forbs, or shrubs may be present in the understory

[a] Trees within a cohort share a common disturbance history; they are those initiated or released after a disturbance (natural or artificial). Tree ages within a cohort may span several decades.

Table 7- Classification rules for forest cover types modeled for sampled subwatersheds in the midscale ecological assessment of the interior Columbia River basin

Forest cover type	SAF cover type(s)	Overstory species composition[a]	Understory species composition[b]
Ponderosa pine	SAF 237	Ponderosa pine,[c] ponderosa pine-Douglas-fir	Grass-forb, shrub, bare ground, ponderosa pine, ponderosa pine-Douglas-fir
Western larch	SAF 212	Western larch, western larch-lodgepole pine, western larch-lodgepole pine-western white pine, western larch-ponderosa pine, western larch-Engelmann spruce, western larch-western white pine	Grass-forb, shrub, or bare ground, western larch-lodgepole pine
Lodgepole pine	SAF 218	Lodgepole pine, lodgepole pine-Engelmann spruce, lodgepole pine-white fir	Grass-forb, shrub, bare ground, lodgepole pine, lodgepole pine-Engelmann spruce, lodgepole pine-white fir, lodgepole pine-ponderosa pine
Douglas-fir	SAF 210	Douglas-fir, Douglas-fir-western larch, Douglas-fir-aspen, Douglas-fir-western white pine, Douglas-fir-lodgepole pine, Douglas-fir-grand fir	Grass-forb, shrub, bare ground, Douglas-fir-western larch, Douglas-fir-lodge-pole pine
Grand fir or white fir, or both	SAF 211 SAF 213	Grand fir or white fir, grand fir-Engelmann spruce, grand fir-ponderosa pine, grand fir-subalpine fir, incense-cedar,[d] grand fir-western white pine, grand fir-western larch	Grass-forb, shrub, bare ground, grand fir or white fir, grand fir-Douglas-fir white fir-Douglas-fir incense-cedar
Pacific silver fir	SAF 226	Pacific silver fir, noble fir	Grass-forb, shrub, bare ground, Pacific silver fir-grand fir, Pacific silver fir-Douglas-fir, Pacific silver fir
Engelmann spruce or subalpine fir, or both	SAF 206	Engelmann spruce-subalpine fir, Engelmann spruce-Douglas-fir, subalpine fir-Douglas-fir subalpine fir-western white pine, subalpine fir-lodgepole pine	Grass-forb, shrub, bare ground, Engelmann spruce- subalpine fir, Engelmann spruce-Douglas-fir
Western hemlock or western redcedar, or both	SAF 224 SAF 227 SAF 228	Western hemlock or western redcedar	Grass-forb, shrub, bare ground, western hemlock or western redcedar
Mountain hemlock	SAF 205	Mountain hemlock, mountain hemlock-Douglas-fir, mountain hemlock-white fir, incense-cedar[e]	Grass-forb, shrub, bare ground, mountain hemlock, mountain hemlock-Douglas-fir, mountain hemlock-white fir, mountain hemlock-lodge pole pine
Whitebark pine or subalpine larch, or both	SAF 208	Whitebark pine or subalpine larch, subalpine fir-subalpine larch	Grass-forb, shrub, bare ground, whitebark pine or subalpine larch
Western white pine or sugar pine, or both	SAF 215[f]	Western white pine or sugar pine, sugar pine-subalpine fir-ponderosa pine	Grass-forb, shrub, bare ground, western white pine and/or sugar pine
Aspen-cottonwood-willow	SAF 217 SAF 222 SAF 235 SAF 233	Hardwoods, maple, birch, aspen, cottonwood, aspen-lodgepole pine	Grass-forb, shrub, bare ground, hardwoods, maple, birch, aspen, cottonwood

APPENDIX E – AERIAL PHOTOGRAPH LANDSLIDE MAPPING METHODOLOGY

Two groups of features were noted based on their relevance to landslide detection: key features and general features. Confidence levels were specified for each identified slide depending on these features. If two or more key features were visible in the aerial photograph, then the mapped slide was assigned a high confidence level. If one key feature and one or more general features were visible, then the mapped slide was assigned a medium confidence level. If two or more general features and no key features were visible, then the mapped slide was assigned a low confidence level. Low confidence level slides may have been caused by events other than landsliding, such as avalanches and rock slides. Slides determined to be caused by an avalanche (no sign of sediment movement) or a rock slide (slides composed almost exclusively of rock and originating from an area of exposed bedrock) were excluded. This general strategy, and the key features listed below are similar to those of Foggin and Rice (1979).

Key Features:
1. Crown Scarp: Distinct crescent-shaped, single or multiple crown scarps, which point down slope (Foggin and Rice, 1979).
2. Slide Runout: Linear-shaped runout path of slide debris below head-scarp.
3. Slide Concavity: The slide cavity is spoon-or bowl shaped (Foggin and Rice, 1979).
4. Debris Mass: The debris mass is often hummocky and may be linear or fan-shaped, depending upon the local slope conditions (Foggin and Rice, 1979).

General Features (Foggin and Rice, 1979):
1. Absence of Vegetation: The vegetation has been removed or buried. In black and white aerial photographs this is denoted by tonal differences, which Foggin and Rice (1979) describe as "generally lighter than its background and recent slides often appear nearly white".
2. Vegetation Change: The vegetation appears to be of a younger age than the surrounding plant community. In black and white aerial photographs, this is denoted by differences in vegetation texture.
3. Linear Form: The disturbed area may extend in linear form from the ridge crest to the channel bottom.
4. Gully Patterns: Rill or gully patterns have developed in the slide cavity or debris mass.

Reference:
Foggin III, G.T. and R.M. Rice, 1979, Predicting Slope Stability from Aerial Photos, *Journal of Forestry*, 152-155.